

Acceptation date : 2019

<https://doi.org/10.20944/preprints201905.0180.v1><https://archimer.ifremer.fr/doc/00498/60946/>

Antagonistic interactions between benzo[a]pyrene and C60 in toxicological response of Marine Mussels

Barranger Audrey ¹, Langan Laura M ¹, Sharma Vikram ¹, Rance Graham A ^{2,3}, Aminot Yann ^{4,5}, Weston Nicola J ³, Akcha Farida ⁵, Moore Michael N ^{1,6,7}, Arlt Volker M ^{8,9}, Kholbystov Andrei N ^{2,3}, Readman James W ⁴, Jha Awadhesh N. ¹

¹ School of Biological and Marine Sciences, University of Plymouth, United Kingdom

² School of Chemistry, University of Nottingham, University Park, Nottingham, NG7 2RD, United Kingdom

³ Nanoscale and Microscale Research Centre, University of Nottingham, University Park, Nottingham, NG7 2RD, United Kingdom

⁴ Centre for Chemical Sciences, University of Plymouth, Plymouth, United Kingdom

⁵ Ifremer, Laboratory of Ecotoxicology, Nantes, France

⁶ Plymouth Marine Laboratory, Prospect Place, The Hoe, Plymouth, United Kingdom

⁷ European Centre for Environment & Human Health (ECEHH), University of Exeter Medical School, Knowledge Spa, Royal Cornwall Hospital, Truro, Cornwall, United Kingdom

⁸ Analytical and Environmental Sciences Division, King's College London, MRC-PHE Centre for Environmental & Health, London, United Kingdom

⁹ NIHR Health Protection Research Unit in Health Impact of Environmental Hazards at King's College London in partnership with Public Health England, London, United Kingdom

Email addresses : audrey.barranger@univ-rennes1.fr ; laura.langan@plymouth.ac.uk ; vikram.sharma@plymouth.ac.uk ; graham.rance@nottingham.ac.uk ; yann.aminot@ifremer.fr ; nicola.weston@nottingham.ac.uk ; farida.akcha@ifremer.fr ; mnm@pml.ac.uk ; volker.arlt@kcl.ac.uk ; andrei.khlobystov@nottingham.ac.uk ; james.readman@plymouth.ac.uk ; a.jha@plymouth.ac.uk

Abstract :

This study aimed to assess the ecotoxicological effects of the interaction of fullerene (C60) and benzo[a]pyrene (B[a]P) on the marine mussel, *Mytilus galloprovincialis*. The uptake of nC60, B[a]P and mixtures of nC60 and B[a]P into tissues was confirmed by GC-MS, LC-HRMS and ICP-MS. Biomarkers of DNA damage as well as proteomics analysis were applied to unravel the toxic effect of B[a]P and C60. Antagonistic responses were observed at the genotoxic and proteomic level. Differentially expressed proteins (DEPs) were only identified in the B[a]P single exposure and the B[a]P mixture exposure groups containing 1 mg/L of C60, the majority of which were down-regulated (~52%). No DEPs were identified at any of the concentrations of nC60 ($p < 0.05$, 1% FDR). Using DEPs identified at a threshold of ($p < 0.05$; B[a]P and B[a]P mixture with nC60), gene ontology (GO) and Kyoto encyclopedia of genes and genomes (KEGG) pathway analysis indicated that these proteins were enriched with a broad spectrum of biological processes and pathways, including those broadly associated with protein processing, cellular processes and environmental information processing. Among those significantly enriched pathways, the ribosome was consistently the top enriched term irrespective of treatment or concentration and plays an important

role as the site of biological protein synthesis and translation. Our results demonstrate the complex multi-modal response to environmental stressors in *M. galloprovincialis*.

Keywords : Trojan Horse effect, B[a]P, nC60, co-exposure, Mussels, DNA damage, proteomics

48 1. Introduction

49 There have been concerns regarding the potential for manufactured nanomaterials to cause
50 unpredictable environmental health or hazard impacts, including deleterious effects across differing
51 organismal levels, for over a decade. Despite numerous years of study, it is still unclear at what
52 quantity manufactured nanomaterials can be found in the aquatic environment, along with their fate,
53 potential bioavailability and subsequent hazardous effects to biological systems. This is surprising
54 given the growing concern in the field of aquatic toxicology regarding their availability and potential
55 toxicity [1]. Fullerenes are the smallest known stable carbon nanostructures and lie on the boundary
56 between molecules and nanomaterials, with fullerenes generally exhibiting strong hydrophobicity in
57 aqueous media [2]. Buckminsterfullerene (C_{60}) is the only readily soluble carbon nanostructure,
58 although graphene is dispersible in specific organic solvents [3]. Non-functionalised C_{60} possesses a
59 measurable, but extremely low solubility in water (1.3×10^{-11} ng/mL), but can exist in the aqueous
60 phase as aggregates (nC_{60}) [4] and is quantifiable in aqueous environmental samples [5]. nC_{60} can be
61 formed in water when fullerenes are released into the aquatic environment, increasing the transport
62 and potential risk of this nanomaterials to the ecosystem ecology.

63 The toxicity associated with C_{60} is controversial and largely unclear [6]. The ability of C_{60} to both
64 generate and quench reactive oxygen species (ROS) has recently been recognised as a particularly
65 important property in the interaction of fullerenes with biological systems [7], with many aquatic
66 studies demonstrating that fullerenes are capable of eliciting toxicity via oxidative stress [8–10].
67 Numerous studies have investigated the beneficial and toxicological effects of fullerenes [11–17].
68 However, the toxicity of nanomaterials has been shown to be dependent on numerous factors,
69 including surface area, chemical composition and shape [18,19]. In specific cases, such as aqueous
70 fullerenes (nC_{60}), the physiochemical structure is influenced by different preparation methods
71 [15,20,21]. Altered physiochemical properties induced through the different methods of solubilisation
72 have been shown to profoundly influence the observed toxicological effects of fullerene exposure,
73 thus making a consensus assessment of environmental toxicity difficult [20]. While the environmental
74 toxicity of fullerenes is still being investigated, an emerging concern is whether fullerene aggregates
75 can act as contaminant carriers (Trojan Horse effects) in aquatic systems, and whether this confirms
76 the reduction or enhancement of toxicity with these compounds. Current evidence suggests a mixture
77 of effects dependent on chemical properties. Under combined aquatic exposure conditions (viz. nC_{60}
78 and contaminant), it has been demonstrated that 17α -ethinylestradiol (EE2) has a decreased
79 bioavailability [14], altered toxicity [11,22] and localised increases in mercury bioavailability [23].
80 Finally, when compared to other anthropogenic contaminants, Velzeboer et al. established that the
81 absorption of polychlorinated biphenyls (PCBs) to nC_{60} was 3-4 orders of magnitude stronger than to
82 organic matter and polyethylene [24]. This enhanced absorption and modifications to toxicity
83 responses may have significant impacts on the fate, transport and bioavailability of co-contaminants
84 already in the aquatic environment. However, more research is necessary to establish which co-
85 contaminants bioavailability is impacted when co-exposed with nC_{60} .

86 The aquatic environment is often the ultimate recipient of an increasing range of anthropogenic
87 contaminants, and likely in all probable combinations. Organisms which are exposed to complex
88 mixtures of differing compounds and substances can interact in many ways to induce biological
89 responses be it additively, synergistically or antagonistically. These interactions can and do change
90 the organismal response compared with single compound exposures [2,25,26]. Bivalves have highly
91 developed processes for the cellular internalization of nano- and microscale particles (viz.
92 endocytosis and phagocytosis) that are integral to key physiological functions such as cellular
93 immunity [27]. These organisms are also useful bio-indicators because as suspension feeders they
94 filter large volumes of water which facilitates uptake and bio-concentration of toxic chemicals [28],
95 in addition to microalgae, bacteria, sediments, particulates and natural nanoparticles. This high
96 filtration rate has been shown to be associated with the high potential accumulation of different
97 chemicals in their tissues. A variety of mussel species have been used to elucidate both physiological
98 and molecular mechanisms of action to nanoparticles [29,30] making them an ideal model to
99 investigate how organisms respond to environmental stressors such as chemical mixtures [27]. This

100 study aims to evaluate the interactions between nC_{60} aggregates and the carcinogen benzo[a]pyrene
101 (B[a]P) using marine mussels. A set of biomarkers or biological responses including proteomic
102 analysis were employed to better understand cellular response to single (viz. B[a]P and C_{60} fullerene)
103 and combined exposures.

104 2. Materials and Methods

105 2.1. Animal collection and husbandry

106 Mussels (*M. galloprovincialis*; 45-50 mm) were collected from the intertidal zone at Trebarwith
107 Strand, Cornwall, UK (50° 38' 40" N, 4° 45' 44" S) in October 2016. The site has previously been used
108 as a reference location for ecotoxicological studies and is considered relatively clean with minimum
109 presence of disease [31,32]. Following collection, mussels were transported to the laboratory in cool
110 boxes and placed in an aerated tank at a ratio of 1 mussel L⁻¹ with natural seawater from Plymouth
111 Sound (filtered at 10 µm). Mussels were maintained at 15°C, fed with micro-algae (*Isochrysis galbana*,
112 Interpret, UK) every 2 days with a 100 % water change 2 h post feeding.

113 2.2. Preparation of stock solutions

114 2.2.1. Fullerenes (C_{60})

115 C_{60} and $Er_3N@C_{80}$ were obtained from Sigma Aldrich UK and Designer Carbon Materials Ltd.,
116 respectively. In order to better replicate the conditions of the experiment during analysis, 2 mussels
117 were maintained in 2-L glass beakers for 24 hrs with natural seawater from Plymouth Sound (filtered
118 at 10 µm). Subsequently, fullerenes (1 mg) were added to the mussel-exposed seawater (10 mL) and
119 the suspension homogenised by ultrasonication (Langford Sonomatic 375, 40 kHz) for 1 hr at room
120 temperature. The suspension was allowed to settle for at least 4 hrs at room temperature prior to
121 analysis of the aggregate size. Dynamic light scattering (DLS) was performed using a Malvern
122 Zetasizer Nano-ZS at room temperature. Quoted values are the average of 3 measurements. Bright
123 field transmission electron microscopy (TEM) and dark-field scanning transmission electron
124 microscopy (STEM) were performed using the JOEL 2100+ microscope operated at 200 keV. Energy
125 dispersive X-ray (EDX) spectra were acquired using an Oxford Instruments INCA X-ray
126 microanalysis system and processed using Aztec software. Samples were prepared by casting several
127 drops of the respective suspensions onto copper grid-mounted lacey carbon films.

128 2.2.2. Benzo[a]pyrene (B[a]P)

129 B[a]P (Sigma Aldrich UK) is not water soluble and was previously dissolved in dimethyl
130 sulfoxide (DMSO) after having determined its solubility limit. Chemical solutions were prepared so
131 that the DMSO concentration in the sea water was 0.001%.

132 2.3. *In vivo* exposure of *M. galloprovincialis* to B[a]P and C_{60} : Experimental design

133 Following depuration, mussels were separated (2 per beaker) into 2 L glass beakers containing
134 1.8 L of seawater and allowed to acclimatize for 48 h. A photoperiod of 12 h light: 12 h dark was
135 maintained throughout the experiment. Oxygenation was provided by a bubbling system. Seawater
136 was monitored in each of the beakers by measuring salinity ($36.45 \pm 0.19\text{‰}$). Mussels were exposed
137 for 3 days with no water changes to B[a]P (5, 50 and 100 µg/L), C_{60} alone (0.01, 0.1 and 1 mg/L) and a
138 combination of B[a]P (5, 50 and 100 µg/L) and C_{60} (1 mg/L). Control groups received only DMSO at the
139 same concentrations as used in the other exposure groups (0.001 % DMSO). A total of 26 individuals
140 were used per treatment. Following exposure, tissue samples were collected as follows: gill and
141 digestive gland (DG) tissue was collected from 3 mussels for chemical analysis, digestive tissue was
142 collected from 9 mussels and pooled (3 mussels per one biological replicate) for shotgun proteomics,
143 DG tissue from 10 mussels was collected for comet assay and DNA adducts, with a further 5 DG

144 collected for DNA oxidation. Water samples from 3 beakers were randomly collected during each
145 treatment for B[a]P and C₆₀ analyses.

146 2.4. GC-MS analyses of B[a]P in water and tissue

147 Water and tissue extracts were analysed using an Agilent Technologies 7890A Gas
148 Chromatography (GC) system interfaced with an Agilent 5975 series Mass Selective (MS) detector as
149 described in [33].

150 2.5. Analyses of C₆₀ in water and tissue

151 The analyses of C₆₀ were performed on the toluene extracts common to the B[a]P analyses. The
152 water extracts were analysed with an Agilent 1100 high-performance liquid chromatography–
153 ultraviolet-visible instrument (HPLC-UV). The separation was performed on a Shimadzu XR-ODS
154 column (particle size 2.2 μm, 3.0 × 50 mm) using an acetonitrile–toluene gradient starting at 40%
155 toluene, at a flow rate of 1 mL/min and a column temperature set at 40 °C. The detection wavelength
156 was set at 330 nm and the fullerene absorption at maximum. Quantification was performed by
157 external calibration using authentic fullerene standards. Because of their lower concentrations, the
158 tissue extracts were analysed by ultrahigh performance liquid chromatography coupled with high
159 resolution mass spectrometry following a protocol adapted from [34].

160 2.6. Proteomics

161 2.6.1. Sample collection and quality check

162 Tissue was removed from the -80 °C, weighed (100 mg) and twice washed in PBS prior to being
163 homogenised on ice for 60 s in RIPA buffer. The lysed homogenate was centrifuged at 14,000 RPM
164 for 60 min at 4 °C, the supernatant collected and aliquoted. Protein concentration was determined
165 using the Pierce BCA protein assay kit (Thermo Scientific) according to manufacturers instructions
166 with bovine serum albumin as standard. Reproducibility of protein extraction was carried out using
167 SDS-PAGE. Briefly, 100 μg of protein from each sample was loaded on a polyacrylamide gradient gel
168 (4-12 %) and stained with Coomassie protein stain (Expedeon, UK) and destained with ELGA water.
169 Quality checked protein samples were then processed for downstream LC-MS analysis.

170 2.6.2. Sample preparation for LC-MS

171 Equal amounts of intestinal protein (100 μg) were processed using the Filter Aided Sample
172 Preparation (FASP) method as described by [35]. The digested proteins were subsequently purified
173 using the STAGE tip procedure as previously described [36]. Tryptic peptides were analysed using
174 liquid chromatography-mass spectrometry (LC-MS).

175 2.6.3. Mass spectrometry

176 Peptides were separated on a Dionex Ultimate 3000 RSLC nano flow system (Dionex, Camberly,
177 UK) and analysed as described in [37].

178 2.6.4. Analysis

179 *Peptide identification and quantification.* Data analysis and quantification was performed using R
180 (Version 3.5.0)[38]. Thermo .raw files were imported into ProteoWizard [39] and converted to .mzML
181 format before identification using the MS-GF+ algorithm which is implemented in R via the
182 MSGFplus package [40]. MS-GF+ was chosen due to its known sensitivity in identifying more
183 peptides than most other database search tools and its ability to work well with diverse types of
184 spectra, configurations of instruments and experimetal protocols [41]. The protein database utilised
185 in this study consisted of the UniProt KnowledgeBase (KB) sequences from all organisms from the
186 taxa Mollusca, sub category Bivalvia (84,410 sequences released 1/10/2018). This was cocatenated
187 with a common contaminants list downloaded from ftp://ftp.thegpm.org/f_asta/cRAP (Version:

188 January 30th, 2015) using the R package seqRFLP [42]. Searches were carried out using the following
189 criteria: mass tolerance of 10 ppm, trypsin as the proteolytic enzyme, maximum number of cleavage
190 sites = 2 and cysteine carbamidomethylation and oxidation as a fixed modification. Target decoy
191 approach (TDA) was applied as it is the dominant strategy for false discovery rate (FDR) estimation
192 in mass-spectrometry-based proteomics [43]. A 0.1 % peptide FDR threshold was applied in
193 accordance with standard practice, with a 1 % protein FDR applied after protein identification (via
194 aggregation). The resulting .mzid files were converted to MSnSet and quantified using label free
195 spectral counts. The mass spectrometry proteomics data have been deposited to the
196 ProteomeXchange Consortium [44] via the PRIDE [45] partner repository with the dataset identifier
197 PXD013805 and 10.6019/PXD013805.

198
199 *Data processing and quantification.* Data processing was under taken as follows: each sample was
200 run individually and then regionally combined before all samples were amalgamated into a large
201 dataset. Quantification of proteins occurred via spectral index (SI) [46]. For identification of proteins,
202 the common practice of requiring three peptides per protein was used in order to reduce the number
203 of false positives [47]. Peptides were subsequently aggregated using sum and the protein intensities
204 scaled based on the actual number of proteins summed. Mussel samples were grouped based on
205 biological replicate, exposure and concentration and the resulting data filtered to keep proteins which
206 were identified in more than two biological replicates. To quantitatively describe reliable and
207 biologically relevant protein expression changes based on single exposure to B[a]P, C₆₀ or to a
208 combination of the two, the data analysis was split into three distinct sections. As per recent
209 recommendations, normalisation was carried out first [48]. Based on systematic evaluations of
210 normalisation methods in label free proteomics, normalisation between technical replicates was
211 carried out using variance stabilization normalisation (Vsn) [49]. Based on a study by Lazar et al. [48],
212 it was hypothesized the most likely cause of missing values will be due to a mixture of MAR (missing
213 at random), MCAR (missing completely at random) and MNAR (missing not at random) data. As
214 such, missing value imputation was carried out using a mixed methodology in the form of KNN (K
215 nearest neighbours, biological replicates) and QRILC (left censor method for MNAR data; whole
216 dataset) [50,51]. Following normalisation, differential expression was carried out using msmsTests
217 [52] with p value less than 0.05 considered significant and Q-values (FDR: < 1%) calculated for p-
218 value target matches with the Benjamini-Hochberg procedure. Enrichment of function among up- or
219 down-regulated proteins was calculated using GOfuncR using gene ontologies associated with
220 differentially expressed proteins (P-adj = 0.01, calculated using Benjamini-Hochberg method and q-
221 value = 0.05). KEGG analysis was carried out on the identified unique proteins per treatment (p < 0.05)
222 using the clusterProfiler package [53]. KEGG annotation was performed using GhostKOALA [54]
223 and pathways with significant enrichment identified using ClusterProfiler (hypergeometric test, q <
224 0.05 following Benjamini correction). Unique and common proteins based on toxicant were
225 graphically represented through Venn diagrams with the software Venny
226 (<http://bioinfogp.cnb.csic.es/tools/venny/index.html>) [55]. The R script outlining project analysis for
227 this study can be found in supplementary materials (R script S1).

228 2.7. DNA damage

229 2.7.1. Measurement of 8-oxodGuo levels using HPLC/UV-ECD

230 DNA extraction was performed using 20 mg of digestive gland tissue according to the chaotropic
231 NaI method derived from Helbock et al. [56], slightly modified by Akcha et al. [57]. 8-oxodGuo levels
232 were determined by HPLC (Agilent 1200 series) coupled to electrochemical (Coulchem III, ESA) and
233 UV (Agilent 1200 series) detection as described in [58]

234 2.7.2. Comet Assay

235 The comet assay on digestive gland tissue was performed as previously described in [33].

236 2.7.3. DNA adducts

237 For each sample, DNA from gills and DG tissues was isolated using a standard phenol-
 238 chloroform extraction procedure. We used the nuclease P1 enrichment version of the thin-layer
 239 chromatography (TLC) ³²P-postlabelling assay [59] to detect BaP-derived DNA adducts (i.e. 10-
 240 (deoxyguanosin-*N*²-yl)7,8,9-trihydroxy-7,8,9,10-tetrahydro-BaP [dG-*N*²-BPDE]). The procedure was
 241 essentially preformed as described [59]. After chromatography, TLC sheets were scanned using a
 242 Packard Instant Imager (Dowers Grove, IL, USA) and DNA adduct levels (RAL, relative adduct
 243 labelling) were calculated as reported [60]. An external BPDE-modified DNA standard was used as
 244 a positive control [61].

245 2.8. Confirmation of uptake of fullerenes by mussels

246 2.8.1. Experimental design

247 Mussels were exposed to a single treatment, 1 mg/L Er₃N@C₈₀ for 3 days (static exposure). For
 248 each treatment (control and labelled fullerenes), 2 mussels were exposed into 2 L glass beakers
 249 containing 1.8 L of seawater.

250 2.8.2. Bulk spectroscopic analysis

251 For the determination of erbium concentration in the digestive gland, 2 mussels per treatment
 252 were analysed using an X Series II ICP-MS (Thermo Fisher Scientific Inc., Waltham, MA, USA) with
 253 PlasmaLab software (Thermo Fisher Scientific Inc., Waltham, MA, USA) as described in [32].

254 2.8.3. Mussel sectioning and electron microscopy analysis

255 Following the exposures detailed above, a small piece (~5 mm²) was dissected out of the centre
 256 of the digestive gland and fixed in 2% paraformaldehyde, 2.5% glutaraldehyde, 2.5% NaCl, 2mM
 257 CaCl₂ in 0.1M PIPES, pH 7.2 for 3h. The tissue was then stored in 2.3 M sucrose (in 0.1M PIPES) until
 258 analysis. Two mussels were analysed per treatment. Electron transparent sections for STEM analysis
 259 were prepared by cutting ~1 mm² pieces from the washed whole tissues and sectioning to a thickness
 260 of ~180-200 nm at -80 °C using the RMC Products PowerTome with the CR-X cryochamber. The cross-
 261 sections were transferred onto copper-grid mounted graphene oxide films using the Tokuyasu
 262 technique and imaged in dark field STEM using the JOEL 2100+ microscope operating at 200 keV.

263 2.9. Statistical analysis

264 Statistical tests were conducted using R software [62]. Normality and variance homogeneity
 265 were evaluated using Lilliefors's test and Bartlett's test, respectively. When necessary, raw data were
 266 mathematically transformed (Ln) to achieve normality before proceeding with an ANOVA. When
 267 significant, a posteriori Tukey test was performed. When data could not be normalized, statistical
 268 differences between treatments were tested using the non-parametric Kruskal-Wallis test.

269 2.9.1. Analysis of interactions

270 Further analysis of the combined effects of C₆₀ and BaP on DNA Damage (based on Comet
 271 Assay) was performed by calculating the Interaction Factor (IF) in order to test for evidence of
 272 additivity, synergism and antagonism [63–65]:

$$\begin{aligned}
 273 & \\
 274 & \text{IF} = (G_{(\text{C}_{60} + \text{BaP})} - C) - [(G_{(\text{C}_{60})} - C) + (G_{(\text{BaP})} - C)] \\
 275 & = G_{(\text{C}_{60} + \text{BaP})} - G_{(\text{C}_{60})} - G_{(\text{BaP})} + C \quad (\text{Equation 1}) \\
 276 & \text{SEM}_{(\text{IF})} = \sqrt{(\text{SEM}_{(\text{C}_{60} + \text{BaP})}^2 + \text{SEM}_{(\text{C}_{60})}^2 + \text{SEM}_{(\text{BaP})}^2 + \text{SEM}_{(\text{C})}^2)} \quad (\text{Equation 2}) \\
 277 & \\
 \end{aligned}$$

278 Where IF is the interaction factor: negative IF denotes antagonism, positive IF denotes
 279 synergism, and zero IF denotes additivity. G is the mean cell pathological reaction to toxicants (BaP,

280 C_{60} and BaP + C_{60}), C is the mean cellular response under control conditions. SEM(x) is the standard
281 error of the mean for group X. Results were expressed as IF, and the 95% confidence limits were
282 derived from the SEM values.

283 In order to test the mixture IF values against predicted additive values (assumed to have an IF =
284 0), the predicted additive mean values (A) were calculated:

$$285 \quad A = (G_{(C_{60})} - C) + (G_{(BaP)} - C) \quad (\text{Equation 3})$$

286
287
288 The Pythagorean theorem method for combining standard errors was used to derive combined
289 standard errors for the predicted mean additive values (A) of C_{60} and BaP
290 ([http://mathbench.org.au/statistical-tests/testing-differences-with-the-t-test/6-combining-sds-for-](http://mathbench.org.au/statistical-tests/testing-differences-with-the-t-test/6-combining-sds-for-fun-and-profit/)
291 [fun-and-profit/](http://mathbench.org.au/statistical-tests/testing-differences-with-the-t-test/6-combining-sds-for-fun-and-profit/)). The standard errors for the three C_{60} and BaP treatments (predicted additive) were
292 derived using the following equation:

$$293 \quad SEM_{(add)} = \sqrt{SEM^2_{(C_{60})} + SEM^2_{(BaP)} + SEM^2_{(C)}} \quad (\text{Equation 4})$$

294
295
296 This enabled the 95% confidence limits to be derived for the predicted additive values. The
297 confidence limits were used to test the predicted additive values having an IF = 0 against the IF values
298 for the mixtures.

299 3. Results

300 3.1. Characterization of C_{60} in seawater

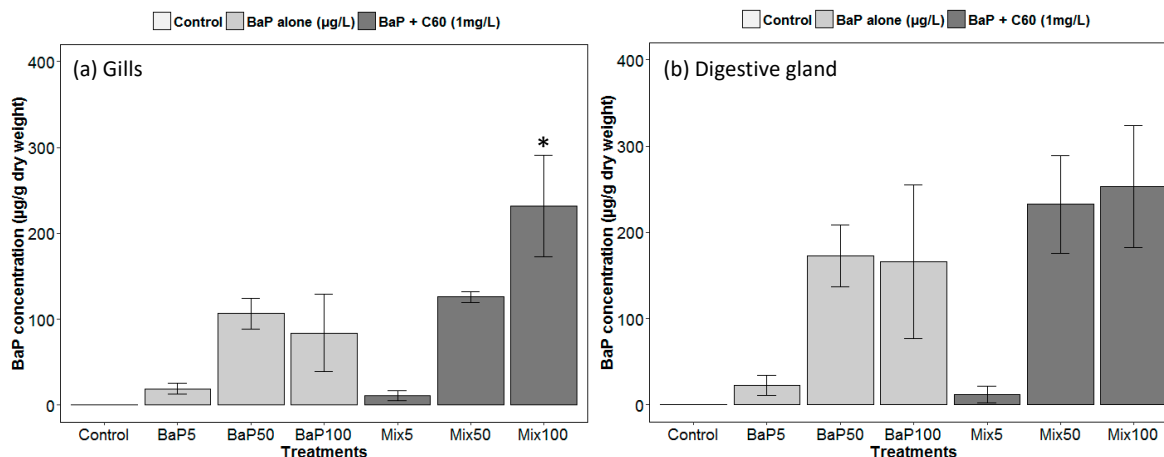
301 Dynamic light scattering and electron microscopy analysis (Figure S1-3 and Table S1) of C_{60}
302 dispersed in mussel-exposed seawater (~100 $\mu\text{g/mL}$) with brief ultrasonication followed by
303 equilibration indicates the formation of stable aggregates measuring 653 ± 87 nm (nC_{60} where
304 $n \sim 2 \times 10^8$) in mean hydrodynamic diameter. No significant change in the size of nC_{60} aggregates was
305 observed upon addition of B[a]P.

306 3.2. Concentration and uptake of B[a]P and C_{60} in seawater and tissue

307 3.2.1. B[a]P

308 Regarding analyses of B[a]P in seawater, nominal concentrations were matched to stock
309 concentrations (Table S2). No difference was observed between the presence or absence of C_{60} . As
310 already established, there was a rapid disappearance of B[a]P over time in seawater and B[a]P
311 accumulated preferentially in the digestive gland tissue. The results are consistent with previous
312 observations in our lab group with a corresponding dose/response profile [33]. There are no
313 significant differences in B[a]P bio-accumulation depending on the presence/absence of C_{60} , except in
314 the gills where a significantly higher uptake is observed in the presence of C_{60} at the highest
315 concentration of B[a]P (Figure 1). In general, high variability would conceal subtle changes.

316



317

318

319

320

Figure 1. GC-MS analyses of B[a]P in (a) gills and (b) digestive gland of *M. galloprovincialis*. Asterisks indicate the statistical differences observed between control and exposed groups. (*) $p < 0.05$, (**) $p < 0.01$, (***) $p < 0.001$.

321

3.2.2. Fullerenes (C₆₀)

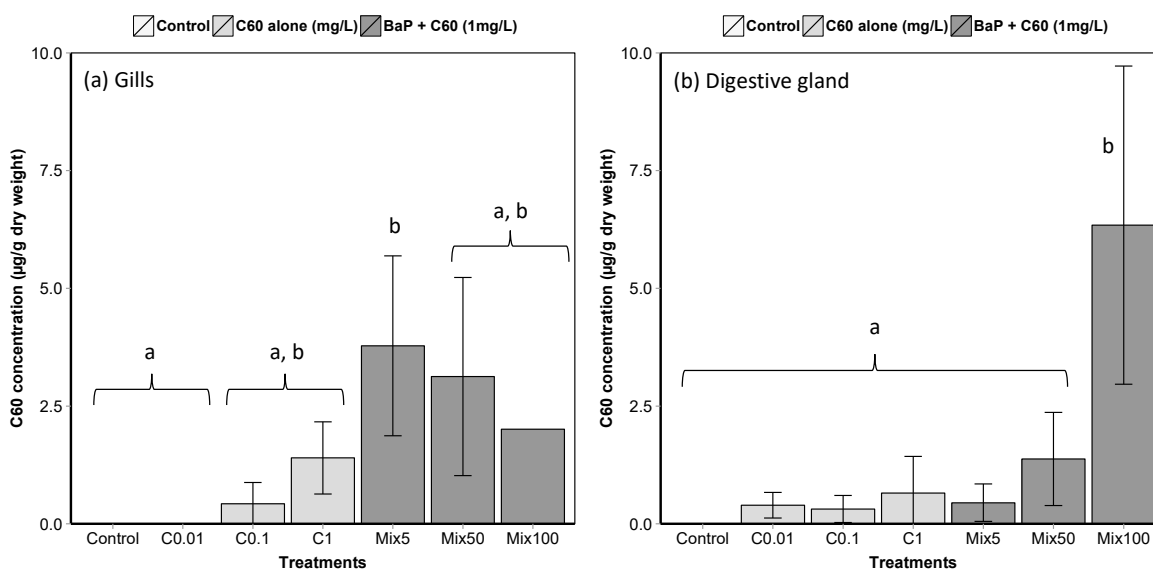
322

A rapid decline in the concentration of C₆₀ in seawater was observed with time, with no quantifiable amounts after day 1 (Table S3). At t_0 , the measured water concentrations are in reasonable agreement with the nominal concentrations (427.6 ± 45.3 , 63.8 ± 11.9 and $7.3 \pm 1.8 \mu\text{g L}^{-1}$ for nominal concentrations of 1000, 100 and $10 \mu\text{g L}^{-1}$ respectively).

326

Low but quantifiable amounts of C₆₀ in *M. galloprovincialis* tissues indicate active uptake, with adsorption on the outside of the tissue ruled out due to external washes with toluene prior to analysis (Figure 2). High variability in C₆₀ concentrations in gills and DG makes difficult to detect difference in accumulation between treatments.

329



330

331

332

333

334

Figure 2. LC-MS analyses of C₆₀ in *M. galloprovincialis* (a) gills and (b) digestive gland (means \pm SE). Data marked with different letters differed significantly (Tukey post-hoc test; $p < 0.05$). An analytical problem led to the loss of two samples of the gills from mussels exposed to Mix100 explaining the absence of standard error.

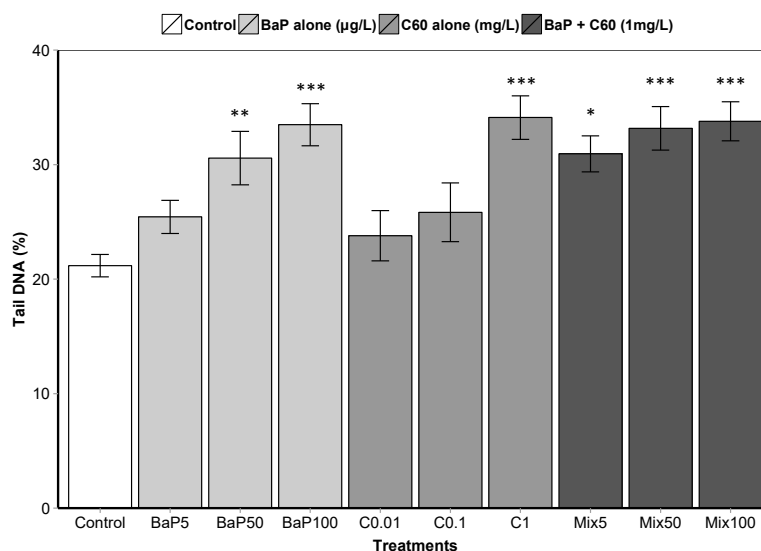
335

3.3. Genotoxicity of B[a]P and C₆₀ in the digestive gland of *M. galloprovincialis*

336

3.3.1. DNA strand breaks

337 B[a]P exposure induced DNA damage in the digestive gland at the intermediate and highest
 338 concentrations (50 $\mu\text{g L}^{-1}$ and 100 $\mu\text{g L}^{-1}$) after 3 days of exposure (Figure 3). No effect was observed
 339 at the lowest concentration. Regarding exposure to C₆₀ only, higher DNA strand breaks compared to
 340 the controls were observed only at the highest concentration (1 mg L^{-1} , $p < 0.001$). Lower C₆₀
 341 concentration did not appear to have any genotoxic effects on mussel digestive gland at the
 342 concentrations tested. In mussels exposed to B[a]P + C₆₀, significant higher DNA damage compared
 343 to control were observed at all the tested concentrations.



344

345 **Figure 3.** DNA strand break level following 3 days of exposure to C₆₀, B[a]P and mixture of both in
 346 the digestive gland. Asterisks indicate the statistical differences observed between control and
 347 exposed groups. (*) $p < 0.05$, (**) $p < 0.01$, (***) $p < 0.001$.

348 *Interactions.* Interactions between C₆₀ and B[a]P on DNA damage (Comet assay) are shown in
 349 Table 1. There is evidence of an antagonistic interaction between C₆₀ and B[a]P at the highest
 350 concentration between C₆₀ and B[a]P (Table 1).

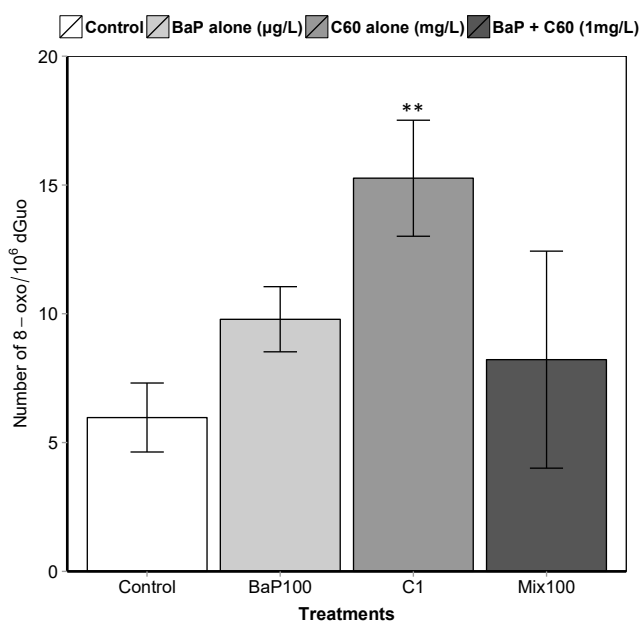
351 **Table 1.** Analysis of combined effects of B[a]P and C₆₀ on DNA damage based on Interaction Factors
 352 (IF)

Treatments	DNA Damage (Comet assay)
<i>BaP 5 $\mu\text{g L}^{-1}$ + C₆₀ 1 mg L^{-1}</i>	-7.48 ± 6.63
<i>BaP 50 $\mu\text{g L}^{-1}$ + C₆₀ 1 mg L^{-1}</i>	-10.39 ± 3.50
<i>BaP 100 $\mu\text{g L}^{-1}$ + C₆₀ 1 mg L^{-1}</i>	$-12.69 \pm 6.05^*$

353

354 3.3.2. DNA oxidation

355 A significant increase ($p = 0.00108$) in 8-oxo-dGuo levels was detected in the digestive gland of
 356 mussels exposed to C₆₀ (15.3 ± 2.3) compared to control (5.9 ± 1.3) (Figure 4). Despite a higher level
 357 of oxidative DNA damage in other treatments compared to control, no significant difference was
 358 observed ($p > 0.05$).



359

360

361

Figure 4. 8-oxodGuo levels in the digestive gland of mussels. Asterisks indicate the statistical differences observed between control and exposed groups. (*) $p < 0.05$, (**) $p < 0.01$, (***) $p < 0.001$.

362

3.3.3. DNA adducts

363

364

Whatever the exposure concentration of B[a]P and mixture of B[a]P and C₆₀, no DNA adducts were detectable in DNA samples from the digestive gland of *M. galloprovincialis*.

365

3.4. Proteomics

366

3.4.1. Identification of differentially expressed proteins

367

368

369

370

371

372

373

374

375

376

377

378

In order to identify differentially expressed proteins in the digestive gland proteome of controls, B[a]P, nC₆₀ and mixture (B[a]P and 1 mg/L nC₆₀), a label free LC-MS/MS approach was used with trypsinised tissue homogenates. Following removal of common contaminants in each dataset, peptide mapping quantified 3125, 3428 and 3475 unique proteins following identification from UNIPROT database distinct to B[a]P, C₆₀ and mixture (B[a]P and 1 mg/L C₆₀) treatments, respectively. Irrespective of treatment, protein sequences from the Pacific oyster *Crassostrea gigas* (Organism ID = 94323) were highly represented in the samples at approximately 38 %, followed by Japanese scallop *Mizuhopecten yessoensis* (Organism ID = 6573) at 34 %. Surprisingly, sequences from the genus *Mytilus* were less represented in the search at approximately 3 % with the Mediterranean mussel *Mytilus galloprovincialis* (Organism ID = 29158) representing approximately 1 % of identified sequences. This may be due to a lack of genomic information available for this genus in the UNIPROT database, even though a genome sequence is available [66].

379

380

381

382

383

384

385

386

387

388

389

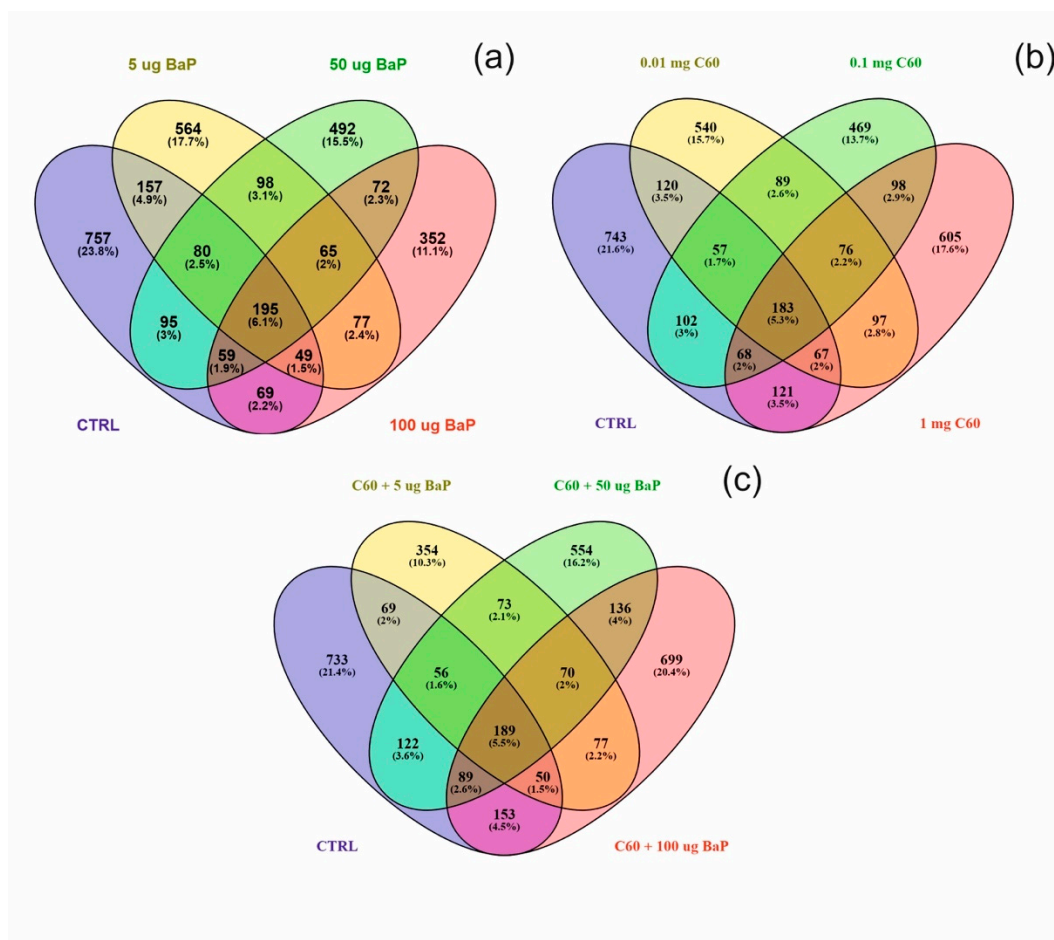
Differentially expressed proteins (DEPs) was determined using a quasi-likelihood GLM. Comparison of each dose per treatment (B[a]P: 5, 50 and 100 $\mu\text{g/L}$, nC₆₀: 0.01, 0.1 and 1 mg/L, and a mixture: 5, 50 and 100 $\mu\text{g/L}$ B[a]P and 1 mg/L nC₆₀) with the control group was visualised using Venn diagrams (Figure 5). Minimal overlap between varying concentrations was observed for the mixture treatment (average of 2 %) (Figure 5c) when compared to B[a]P (Figure 5a, 9 %) or nC₆₀ (Figure 5b, 8 %). Volcano plots were used to visualise statistically significant changes in protein abundance for varying concentrations of the above treatments following comparison to controls (Figure 6). Applying a 1 % FDR threshold, 401 differentially expressed proteins were identified following B[a]P treatment (all concentrations) and 297 differentially expressed proteins were identified following treatment with the mixture of B[a]P and nC₆₀. No differentially expressed proteins ($p < 0.05$) were identified in C₆₀ treated samples. The identified DEPs can be further broken down based on treatment

390 with 42, 50 and 164 DEPs identified at 5, 50 and 100 $\mu\text{g/L}$ B[a]P. Following exposure to a mixture
 391 solution, 95, 108 and 94 DEPs were identified at each concentration respectively (1 mg/L of C₆₀ and 5,
 392 50 and 100 $\mu\text{g/L}$ of B[a]P) with Figure 7 representing a visual comparison of commonalities between
 393 single exposure versus combined exposure. A subset of DEP based on the top 3 unique proteins per
 394 concentration is displayed in Table 2, with the full list of unique proteins and associated p-value and
 395 FDR correction (Spreadsheet S1). The majority of differentially expressed proteins detected in this
 396 study (B[a]P and mixture exposure) were down-regulated (52%) between the treatment and control
 397 conditions irrespective of concentration.

398 3.4.2. GO functional enrichment

399 Gene ontologies were directly annotated using a custom annotation database derived from
 400 UNIPROTKB (bivalvia) with enrichment carried out using GOfuncR. This provides a controlled
 401 vocabulary to describe gene product characteristics in three independent ontologies viz. biological
 402 process, molecular function and cellular components. Based on the R package GOfuncR, 31, 35 and
 403 23 GO nodes were found enriched at a threshold of $p < 0.05$ (FWER correction) following treatment
 404 with B[a]P, C₆₀ or co-mixtures (5 - 100 $\mu\text{g L}^{-1}$ B[a]P and 1 mg L⁻¹ C₆₀). The top GO terms are listed in
 405 Table 3 (threshold set FWER = 0.01), while the full list separated by treatment and concentration can
 406 be found in supplemental material (Spreadsheet S1). Irrespective of treatment, biological process
 407 records the majority of enriched terms.

408



409

410 **Figure 5.** Venn diagram visualising the overlap between the control sample and varying
 411 concentrations of B[a]P (a), C₆₀ (b) or a mixture of the two (5-50-100 $\mu\text{g/L}$ B[a]P 1 mg/L C₆₀) (c)
 412 following exposure for 3 days. Note that overlap is based on a threshold of $p < 0.05$ and does not
 413 include FDR correction.

414
415
416**Table 2.** Significantly expressed proteins of B[a]P, C₆₀ and mixture (5- 100 µg/L and 1 mg/L C₆₀). Species id's are as follows: 6573 = *Mizuhopecten yessoensis*, 6551 = *Mytilus trossulus*, 29159 = *Crassostrea gigas* and 94323 = *Crassostrea ariakensis*.

Treatment	Species	Protein Name	UNIPROTKB	GO annotation	Regulation
B[a]P (5 µg/L)	6573	Arrestin domain-containing protein 3	A0A210PE39		Up
B[a]P (5 µg/L)	6573	Orexin receptor type 2	A0A210PSC6	GO:0004930, GO:0016021	Up
B[a]P (5 µg/L)	6573	Ran-specific GTPase-activating protein	A0A210Q6H5	GO:0005622, GO:0046907	Up
B[a]P (50 µg/L)	6573	5-hydroxytryptamine receptor 1A-alpha	A0A210R4M3	GO:0004993, GO:0005887, GO:0008283, GO:0042310, GO:0046883, GO:0050795	Down
B[a]P (50 µg/L)	6573	Adenylate kinase isoenzyme 5	A0A210QMB2	GO:0005524, GO:0006139, GO:0019205	Up
B[a]P (50 µg/L)	6573	Uncharacterised protein	A0A210Q912		Up
B[a]P (100 µg/L)	6573	Helicase with zinc finger domain 2	A0A210PQ46	GO:0004386, GO:0030374	Up
B[a]P (100 µg/L)	29159	Peroxiredoxin-4	K1QLH0	GO:0005623, GO:0045454, GO:0051920	Up
B[a]P (100 µg/L)	29159	Hypoxia up-regulated protein 1	K1QBF7	GO:0005524	Up
B[a]P (5 µg) + C60 (1 mg/L)	94323	Ras-like GTP-binding protein RHO	H9LJA2	GO:0003924, GO:0005525, GO:0005622, GO:0007264	Up
B[a]P (5 µg) + C60 (1 mg/L)	29159	Zinc finger CCCH domain-containing protein 13	K1PKC9	GO:0046872	Up
B[a]P (5 µg) + C60 (1 mg/L)	29159	Myosin heavy chain, non-muscle (Fragment)	K1QXX7	GO:0003774 GO:0003779, GO:0005524 GO:0016459	Up
B[a]P (50 µg) + C60 (1 mg/L)	6551	Ribosomal protein S20	A0A077H0N2	GO:0003723, GO:0003735, GO:0006412, GO:0015935	Down
B[a]P (50 µg) + C60 (1 mg/L)	6573	Nucleolar and coiled-body phosphoprotein 1	A0A210Q9W0	GO:0005730	Down
B[a]P (50 µg) + C60 (1 mg/L)	29159	Tripartite motif-containing protein 2	K1QBD4	GO:0005622, GO:0008270	Up
B[a]P (100 µg) + C60 (1 mg/L)	6573	Ran-specific GTPase-activating protein	A0A210Q6H5	GO:0005622, GO:0046907	Down
B[a]P (100 µg) + C60 (1 mg/L)	29159	Uncharacterized protein	K1R543		Down

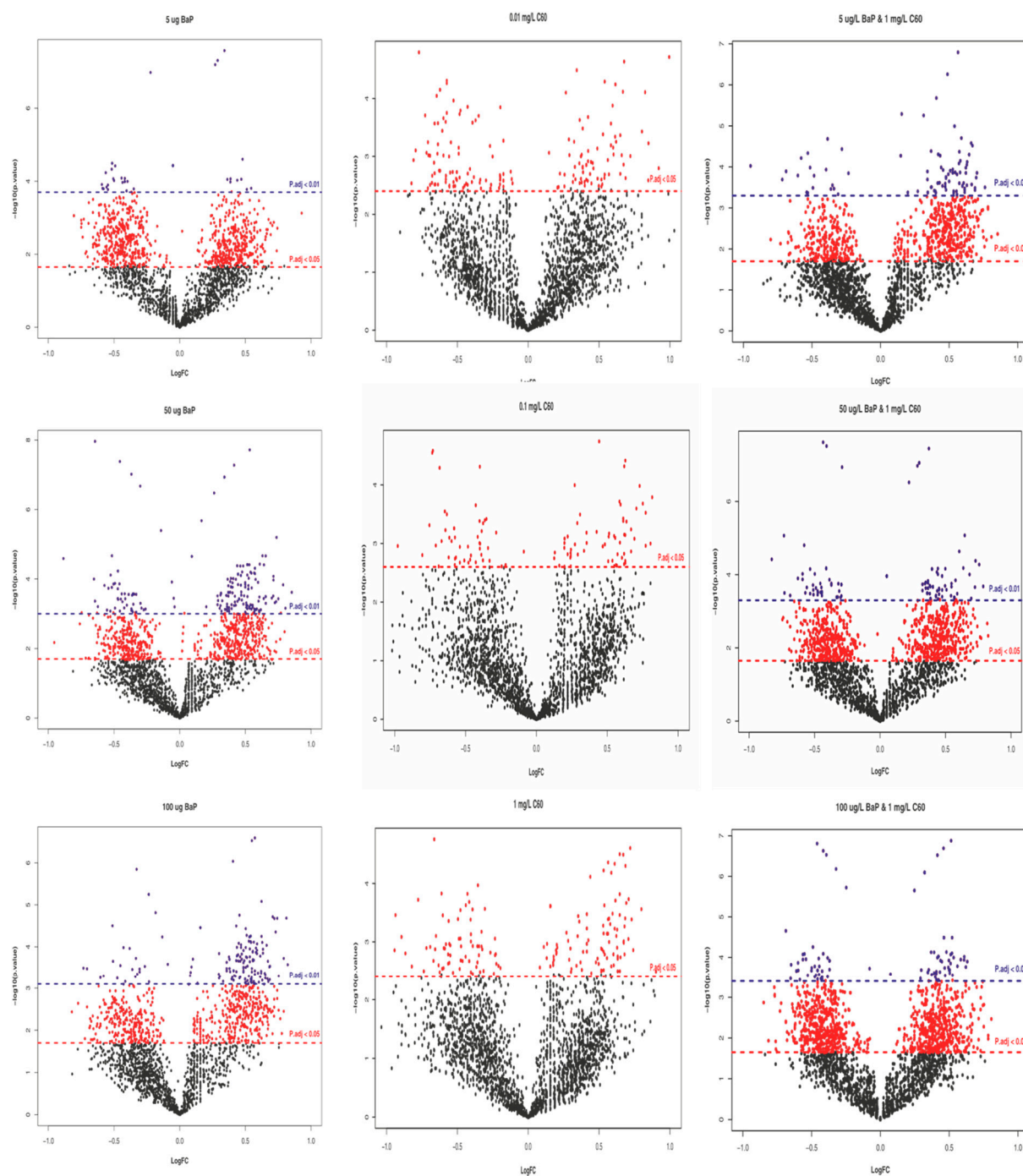
417

418 3.4.3. KEGG pathway enrichment

419 To further analyse the identified proteins per treatment, KEGG pathway analysis was
420 performed. Using the bioconductor package clusterProfiler, protein sequences were assigned to DEPs
421 ($p < 0.05$) and submitted to GhostKoala to obtain KEGG Orthology numbers (KO). In general, 52-56
422 % of entries were successfully annotated with approximately 92 % of annotations associated with the
423 mollusca taxonomy. Variation between enrichment was described per treatment and concentration
424 as follows:

425 **B[a]P:** at 5 $\mu\text{g/L}$ exposure, 52 enriched processes were identified and include ribosome processes
426 (26 genes), thermogenesis (19 genes), protein processing in endoplasmic reticulum (13 genes) and
427 mTOR signalling pathway (9 genes). At 50 $\mu\text{g/L}$ exposure, 38 pathways were enriched and ribosome
428 (26 genes), protein processing in the endoplasmic reticulum (17 genes) and phagosome (13 genes).
429 Finally, at 100 $\mu\text{g/L}$, 26 enriched processes were identified including ribosome (26 genes), RNA
430 transport (16 genes), protein processing in the endoplasmic reticulum (16 genes), biosynthesis of
431 amino acids (16 genes) and endocytosis (15 genes). The mTOR signalling pathway was not enriched
432 at either 50 or 100 $\mu\text{g/L}$.

433



V

434

435

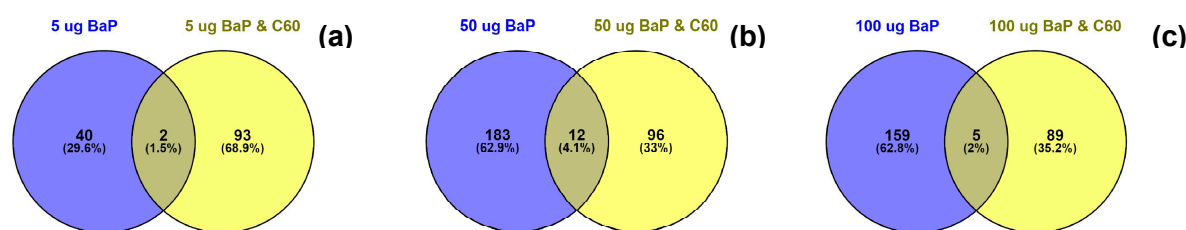
436

437

438

Figure 6. Volcano plots representing the differentially expressed proteins with exposure to B[a]P (a), C₆₀ (b) or a mixture of the two (5-50-100 μ g/L B[a]P 1 mg/L C₆₀) (c). Red dots represent DEPs ($p < 0.05$) with an FDR of 5% while blue dots represent DEPs with an FDR of 1%. Black dots represent unique proteins which are not differentially expressed.

439



440

441 **Figure 7.** Venn diagram visualising the overlap between 5 $\mu\text{g/L}$ (a), 50 $\mu\text{g/L}$ (b) and 100 $\mu\text{g/L}$ (c) of
 442 B[a]P with a mixture solution containing the same B[a]P concentrations in addition to 1 mg/L of C₆₀
 443 following 24 h exposure. Overlap is based on $p < 0.05$ and FDR set at 1 %.

444 **Table 3.** Subset of enriched Gene Ontology (GO) terms with an family wise error (FWER) threshold
 445 of 1 % (or 0.01) following B[a]P (5-100 $\mu\text{g/L}$), C₆₀ (0.01 – 1 mg/L) and a mixture of B[a]P (5-100 $\mu\text{g/L}$)
 446 and C₆₀ (1 mg/L) treatments. Cellular component and biological processes are abbreviated to CC and
 447 BP respectively.

Treatment	Ontology	GO-ID	GO-ID Name	FWER
B[a]P (100 μg)	BP	GO:0006139	Nucleobase-containing compound metabolic process	0.01
B[a]P (100 μg)	BP	GO:0006725	Cellular aromatic compound metabolic process	0.01
B[a]P (100 μg)	BP	GO:0034641	Cellular nitrogen compound metabolic process	0.01
B[a]P (100 μg)	BP	GO:0046483	Heterocycle metabolic process	0.01
B[a]P (100 μg)	BP	GO:0090304	Nucleic acid metabolic process	0.01
B[a]P (100 μg)	BP	GO:1901360	Organic cyclic compound metabolic process	0.01
C ₆₀ (0.01 mg/L)	BP	GO:0000226	Microtubule cytoskeleton organization	0.01
C ₆₀ (0.1 mg/L)	CC	GO:0031974	Membrane-enclosed lumen	0.01
C ₆₀ (0.1 mg/L)	CC	GO:0043233	Organelle lumen	0.01
C ₆₀ (0.1 mg/L)	CC	GO:0070013	Intracellular organelle lumen	0.01

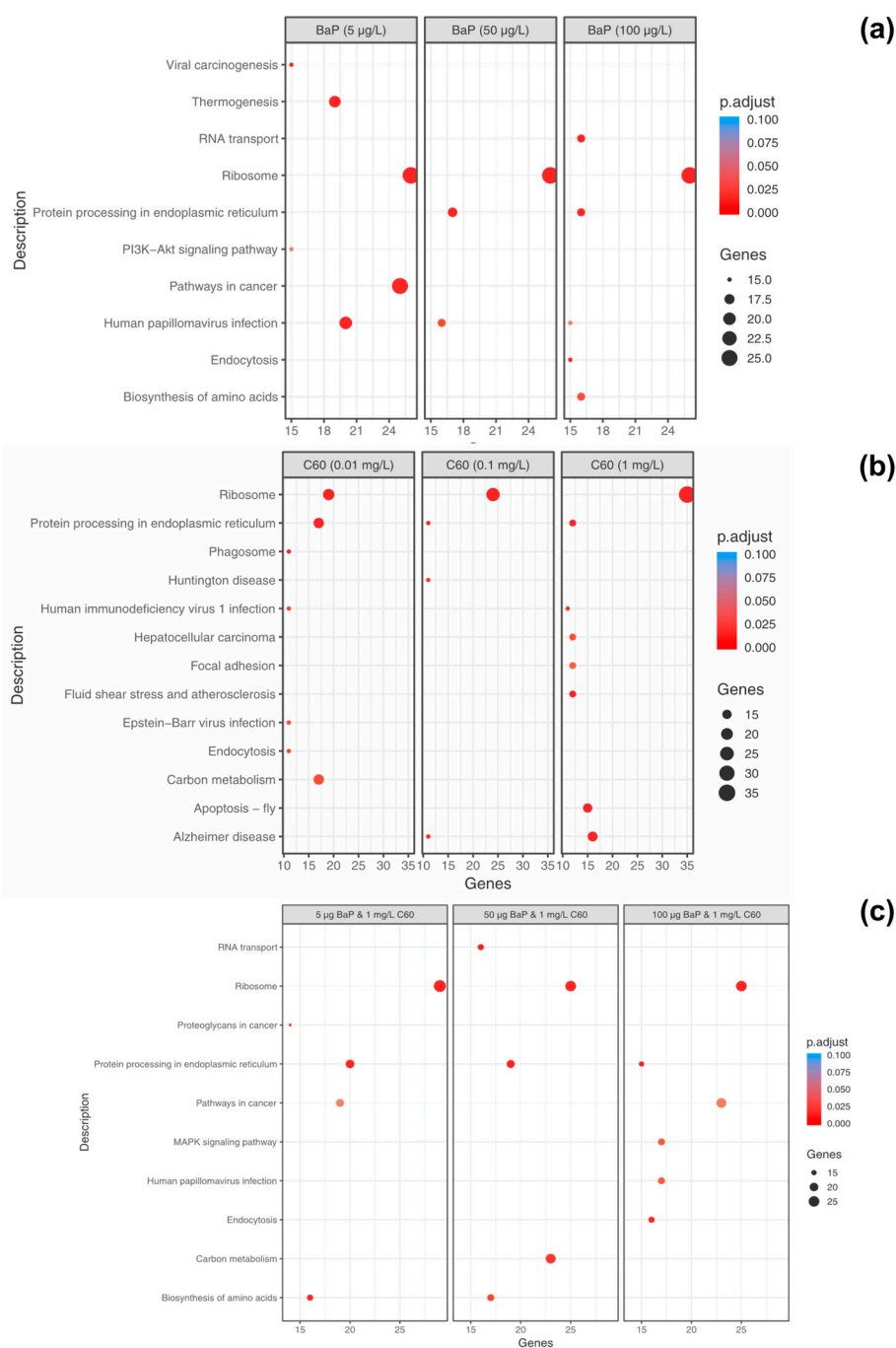
448

449 The majority of enriched pathways identified can be grouped under genetic information
 450 processing, cellular processes, environmental information processing and metabolism. The top
 451 enriched pathways identified per concentration were plotted to identify commonalities and
 452 differences between differing concentrations of B[a]P (Figure 8a) based on genes identified in that
 453 pathway. Interestingly, unique pathways appear to be activated dependent on exposure
 454 concentration, with only the ribosome pathway consistently present and enriched at all

455 concentrations potentially indicating the high degree of translation which may be occurring as a
 456 consequence of PAH exposure.

457 C_{60} ; at 0.01 mg/L exposure, 33 enriched pathways were identified while 12 enriched pathways
 458 were identified at 0.1 mg/L exposure and 35 enriched pathways identified at 1 mg/L exposure ($p <$
 459 0.05, FDR = 5%). The top enriched pathways were illustrated in Figure 8b, with an absence of
 460 enrichment of certain pathways dependent on treatment concentration. For example, thermogenesis
 461 was only enriched at the highest concentration of 1 mg/L with 12 genes identified in the pathway.
 462 The ribosome is the top enriched pathway at all concentrations of C_{60} with 19 genes enriched at 0.01
 463 mg/L exposure, 24 genes enriched at 0.1 mg/L exposure and 35 genes enriched at the highest
 464 concentration of 1 mg/L. This is closely followed by protein processing in endoplasmic reticulum,
 465 which is broadly comparable in terms of genes between 0.01 mg/L (17 genes), 0.1 mg/L (11 genes)
 466 and 1 mg/L (16 genes, Figure 9) exposure. The enriched pathways can be broadly grouped into
 467 predominantly genetic information processing, metabolism and cellular processes.

468

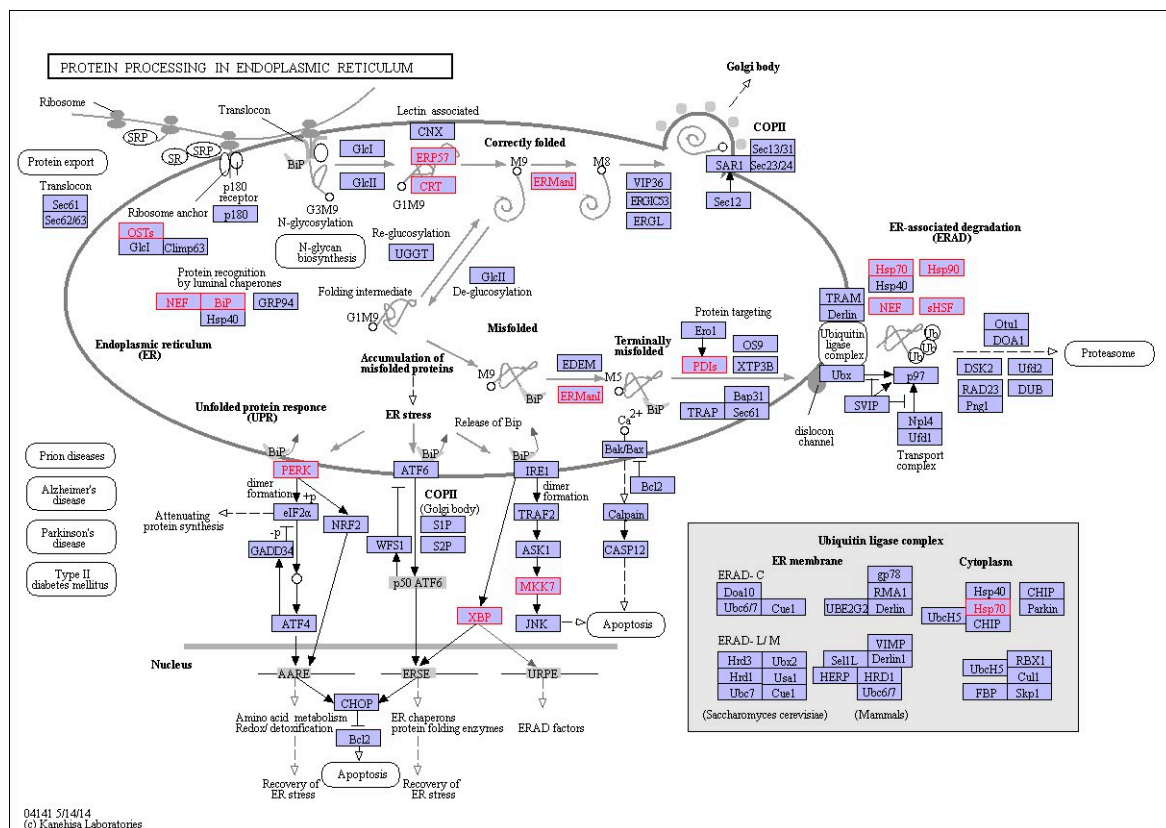


469

470 **Figure 8.** Dotplot of enriched KEGG pathways for DEGs ($p < 0.05$) that were common between
 471 concentrations of B[a]P (a), C₆₀ (b) and a mixture of 5, 50 and 100 $\mu\text{g/L}$ with 1 mg/L C₆₀ (c). Along the
 472 x-axis, genes represent the number of genes identified as enriched in this particular pathway. The size
 473 and colour of each dot represents the gene number and adjustment p based on FDR correction.

474 **Mixtures:** Under mixture scenario, C₆₀ at a constant concentration of 1 mg/L was mixed with 5
 475 $\mu\text{g/L}$, 50 $\mu\text{g/L}$ and 100 $\mu\text{g/L}$ of B[a]P resulting in 50, 38 and 54 enriched pathways respectively. At the
 476 lower mixture concentration of 5 $\mu\text{g/L}$ B[a]P and C₆₀, the top 3 enriched descriptive terms were related
 477 to the ribosome (29 genes), protein processing in endoplasmic reticulum (20 genes) and pathways in
 478 cancer (23 genes). At 50 $\mu\text{g/L}$ B[a]P and C₆₀, the top 3 enriched descriptive terms were related to the
 479 ribosome (23 genes), carbon metabolism (23 genes) and protein processing in endoplasmic reticulum
 480 (19 genes).

481



482 **Figure 9.** Interaction network of differentially expressed genes in the digestive gland of
 483 *M.gallopvinctialis* involved in protein processing in the endoplasmic reticulum during exposure to 1
 484 mg/L nC₆₀. Genes which are differentially expressed during exposure are highlighted in red.
 485

486 Finally, at 100 $\mu\text{g/L}$ B[a]P and C₆₀, the top 3 enriched descriptive terms were related to the
 487 ribosome (25 genes), pathways in cancer (23 genes) and MAPK signalling pathway (17 genes). Key
 488 genes consistently identified in the protein processing in the endoplasmic reticulum (irrespective of
 489 treatment) include *Hsp70*, *Hsp90*, *TRAP*, *PDIs* and *OSTs*. At the highest concentration of B[a]P
 490 and C₆₀, genes identified in pathways in cancer include *GSTs*, *CASP3* and *Wnt*. The top pathways based
 491 on quantity of genes present in the pathway were presented in Figure 8 with clear trends towards an
 492 absence of enrichment in certain pathways based on mixture concentration, e.g. MAPK signalling
 493 which is only present at the top exposure concentration combination.

494 3.5 Analysis of fullerenes (C₆₀) uptake in mussels

495 To provide further insight into the uptake of fullerenes by marine mussels, it was necessary to
496 use a form labelled with a diagnostic marker. In our experiments, we explored the application of the
497 endohedral fullerene Er₃N@C₈₀, fabricated using the trimetallic nitride template (TNT) process, as it
498 represents a good structural analogue to C₆₀, possessing similar surface chemistry, and contains a
499 rare earth element, shielded from the external environment within the fullerene cage, that is not
500 found in nature. The presence of erbium in the mussel digestive gland, as diagnostic of the uptake of
501 labelled fullerenes, was thus quantified using ICP-MS and found with a mean concentration of 151.5
502 µg/kg (236.5 µg/kg and 66.4 µg/kg for each mussel). However, despite an exhaustive electron
503 microscopy investigation of whole and cross-sectioned DG tissues (Figures S4, Supplementary
504 materials), no direct visualisation of labelled fullerenes was observed.

505 4. Discussion

506 Bivalves are ideal organisms for evaluating the adverse effects caused by various environmental
507 stressors including polycyclic aromatic hydrocarbons (PAHs) and nanomaterials. PAHs such as B[a]P
508 have a ubiquitous aquatic distribution and are known to cause several adverse effects in a diverse
509 range of aquatic organisms. While single exposure studies are more common, various bivalve species
510 have already been used as biological models in proteomics to assess the effects of complex mixtures
511 [22,67,68] in addition to other aquatic species [69,70]. Nanomaterials, both as solids and colloids, are
512 ingested by many organisms and bio-accumulate in large quantities, especially in molluscs. The
513 mussel digestive gland is one of the principal detoxification organs with an acknowledged
514 concentration of phase I detoxification enzymes [71]. As such, it is unsurprising that mussel digestive
515 gland has been used as model tissue for eco-toxicological studies of various NPs [72–74], with Di et
516 al. reporting that the digestive gland in *Mytilus edulis* accumulates more C₆₀ than other tissues [72].

517 There is considerable debate in the literature regarding the actual toxicological impact of
518 nanomaterials in the aquatic environment, with fullerene toxicity controversial. In the aquatic system,
519 Kahru et al. compiled fullerene toxicological data for fourteen organisms and classified C₆₀ as "very
520 toxic" [75]. Using mouse and human cell lines, Isakovic et al. demonstrated that pristine C₆₀ and
521 aqueous suspensions of C₆₀ are more toxic than its hydroxylated derivatives [76]. In marked contrast,
522 other studies have demonstrated that pristine C₆₀ has low or limited toxicity to cells and various
523 organisms [10,77–79]. The lack of consensus regarding C₆₀ toxicity may be partly due to limited
524 studies which incorporate both a physiological and ecological approach. As a consequence, little is
525 still known about NP bioavailability, mode of uptake, ingestion rates and actual internal
526 concentrations related to Absorption, Distribution, Metabolism and Excretion (ADME) [27]. Despite
527 the contradictory reports, there is consensus that some nanomaterials may potentially affect
528 biological systems directly but also through interactions with other compounds which may be
529 available in the environment (reviewed in [6]). Studies which investigate co-exposure with carbon-
530 based nano-compounds, such as nanotubes or fullerenes are limited, especially in aquatic systems.
531 Using *Danio rerio* (zebrafish) hepatocytes, Ferreira et al. investigated the co-exposure of C₆₀ with B[a]P
532 and provided evidence of toxicological interactions whereby C₆₀ increased the uptake of B[a]P into
533 cells, decreased cell viability and impaired detoxification responses [69]. While, Baun et al. reported
534 that co-exposure with fullerene C₆₀ enhanced toxicity of phenanthrene to *Daphnia magna* and
535 *Pseudokirchneriella subcapitata* [22]. With respect to B[a]P and C₆₀, Di et al demonstrated organ specific
536 response to both single and combined mixtures with no observation of cytotoxicity and duration
537 dependent and condition specific genotoxic response in *M. galloprovincialis* [72]. Importantly, the
538 observed genotoxic response was reversible after a recovery period. In this study, we add to the
539 growing evidence that toxicity associated with C₆₀ may in fact be related to the nanomaterials ability
540 to act as a vector for other contaminants, and in its aqueous form is not inherently toxic itself.

541 4.1. Chemistry support

542 4.1.1. Accumulation of B[a]P

543 Comparable B[a]P tissue concentrations in the presence or absence of C₆₀ indicate that despite the
544 expected strong sorption of B[a]P on C₆₀ [80], C₆₀-sorbed B[a]P remains bioavailable to *M.*
545 *galloprovincialis*. Changes in the bioavailability of contaminants co-exposed with carbon nanomaterial
546 has been reported, from a decrease in bioavailability [81,82] to its enhancement, also called the
547 “carrier effect” [83,84]. It has been demonstrated that carbon nanopowder helps BaP uptake by
548 zebrafish embryos and very interestingly also affected the distribution of the pollutant in the
549 organism [85]. However, in the same species, in zebrafish larvae it has been shown that bioavailability
550 of 17 α -ethynylestradiol (EE2) was reduced with increasing concentration of nC₆₀ nanoparticles [14].
551 It appears that the bioavailability of nanomaterials and their co-contaminants depends on many
552 factors such as their size, shape, surface coating and aggregation state and on the metabolism of the
553 species investigated [81,86].

554 4.1.2. Accumulation of C₆₀

555 In a previous study in *M. galloprovincialis* [87], mussels exposed to C₆₀ alone showed higher
556 accumulation of C₆₀ in the digestive gland compared to the gill. Interestingly, co-exposure to
557 fluoranthene modified accumulation of C₆₀, with higher accumulation of C₆₀ when animals are
558 exposed to C₆₀ alone compared to combined exposure.

559 When comparing water and tissue concentrations for B[a]P and C₆₀, the bioconcentration
560 observed in our conditions was much lower for C₆₀ compared to B[a]P: the uptake in the DG of
561 mussels exposed to a similar aqueous concentration of B[a]P and C₆₀ was about 2000 times more
562 important for B[a]P. However, non-constant concentrations in the aqueous phase, attributed to
563 sorption and/or sedimentation, did not allow the calculation of bioaccumulation factors, which also
564 requires reaching a steady-state in the tissues. The difference between B[a]P and C₆₀ tissue
565 concentration could also be attributed to different kinetics of uptake, which could only be explored
566 through longer exposure periods and regular sampling. Recent work indicated a continuous increase
567 of C₆₀ concentrations in whole mussels over at least 3 weeks [88].

568 Further confirmation of the accumulation of fullerenes within mussels was afforded by ICP-MS
569 analysis of digestive gland tissues extracted from mussels exposed to Er-labelled fullerenes.
570 However, no evidence for the presence of labelled fullerene aggregates within tissue sections using
571 our novel STEM-EDX approach was afforded, indicating that the fullerenes are likely distributed
572 within the tissues at the near molecular level (i.e. highly dispersed) and therefore below the
573 sensitivity of either microscopy or *in situ* spectroscopy approaches in complex materials such as these.

574 4.2. DNA damage

575 Most of the observed DNA damage will result from oxidative injury by ROS generated by futile
576 cycling of BaP, and also produced by C₆₀ and lipofuscin associated iron [89,90]. According to a
577 review by Johnston et al., fullerene toxicity has been suggested to involve oxidant-driven response
578 and suggests evaluating toxicity by including oxidative stress and related consequences including
579 inflammation or genotoxicity [91].

580 As already observed in [72], mixture did not increase the formation of DNA strand breaks in the
581 digestive gland of *M. galloprovincialis*. Interestingly, the analysis of interactions performed on the
582 comet assay results revealed an antagonistic effect at the highest concentration in the co-exposure
583 treatments. The analysis of oxidative DNA damage through the analysis of 8-oxodGuo confirmed the
584 induction of oxidative damage by C₆₀. The small increase (not significant) of 8-oxodGuo observed for
585 B[a]P treatment could be due to the short exposure time (3 days). In [57], an increase in the level of 8-
586 oxodGuo was observed after 10 days of B[a]P exposure in the digestive gland of *M. galloprovincialis*.
587 In our study, the antagonistic effect observed in the co-exposure treatment at the highest
588 concentration may be caused by a reduction in ROS generation, or more effective scavenging of ROS
589 by C₆₀, when C₆₀ and BaP are present together in close association, as previously described by [9,72].
590 C₆₀ fullerenes are both scavengers and generators of reactive oxygen species (ROS) [92]; and when
591 C₆₀ and BaP are closely associated or bound together within the lysosomal compartment of the mussel
592 digestive cells, their ROS scavenging and generating properties may be altered.

593 4.3. Protein expression profiles

594 Investigations into proteome responses of marine organisms to various stressors is
595 comparatively small when compared to other model laboratory organisms, both aquatic and
596 terrestrial. Proteomic analysis represents a fundamental step in extending understanding of the
597 physiological processes involved in organismal responses to environmental stressors. In addition,
598 proteomics also provides better qualitative data on post-translational modifications without
599 interference from mRNA instability [93]. A major limitation in the field has been the lack of available
600 annotated genomes for a broad diversity of marine organisms. As a consequence, it has been
601 considered a widely under utilised tool [94]. The lack of genome information has not stopped studies
602 on proteome characterisation in bivalvia/mollusca species using broad protein databases limited to
603 either the phylum, class or specific combination of species [95–98]. However, studies investigating
604 proteome response to environmental stressors or injury are less abundant [30,68,99]. In the current
605 study, a label free shot-gun proteomics approach was performed to investigate proteome alterations
606 in the digestive gland of *M. galloprovincialis* following treatment with B[a]P, C₆₀ and a combination of
607 B[a]P with 1 mg/L of C₆₀. In the identification of proteome changes between conditions and
608 contaminants, a default threshold for fold change was not set *a priori* in order to appreciate moderate
609 protein changes. Instead, strict statistical criterion for significance was adopted. Whilst thousands of
610 unique proteins were identified in each treatment, differentially expressed proteins were only
611 identified following treatment with B[a]P and B[a]P in combination with C₆₀. Focusing on B[a]P
612 exposure, proteomic analysis of mussel digestive gland revealed significant differences at all
613 exposure concentrations when compared to the control. Statistically, 42, 195 and 164 proteins were
614 differentially expressed after a 3-day exposure at 5, 50 and 100 µg/L of B[a]P (1% FDR, $p < 0.05$). In
615 comparison, no differentially expressed proteins were identified following a 3 day C₆₀ exposure.
616 However, when B[a]P was co-exposed to C₆₀ (1 mg/L), differentially expressed proteins at the two
617 highest concentrations in the mixture exposure decreased when compared to single exposure (Figure
618 7). This trend towards higher protein alterations in single exposures versus co-exposures suggests a
619 non-additive combine effect and is in agreement with prior studies which reported generally higher
620 protein alterations of B[a]P and Cu under single exposure then when co-exposed together [68]. The
621 data in this study suggests that an interaction occurs between B[a]P and C₆₀ whereby the effect of the
622 mixture is different from the presumption of additivity (were by dose response relationships of
623 mixtures are enhanced in comparison to the individual components) as outlined in Rosa et al [100].
624 In this case, the data suggests an antagonistic relationship between B[a]P and C₆₀ at the higher
625 concentrations of 50 and 100 µg/L. This observation has previously been observed in *Mytilus edulis*
626 digestive gland [72]. However, this trend is not replicated at the lowest concentration of 5 µg/L
627 whereby mixture exposure resulted in higher DEPs than single exposure. This difference in DEPs
628 may potentially be related to reduced accumulation of B[a]P at the higher concentrations due to
629 saturation of mussel tissue and thereby limiting protein changes. In previous studies, increased
630 impact and accumulation of B[a]P at lower concentrations in *M. galloprovincialis* has been attributed
631 to tissue saturation [101]. The increase in differentially expressed proteins at the lower concentration
632 may also reflect the inability of membrane transporters such as p-glycoprotein to efflux this particular
633 nanoparticle [102] and as such acts to bypass typical protective mechanisms initiated to protect the
634 organism from PAH stress.

635 The ability of a stress organism to adjust its cellular processes via transcriptional and
636 subsequently proteomic processes allows it where possible to minimise cellular damage, which may
637 lead to organism death. GO analysis revealed 30 enriched proteins following B[a]P exposure, 42
638 following C₆₀ exposure and 31 in the mixture exposure. The response of *M. galloprovincialis* to B[a]P
639 is characterised by a predominant enrichment of Biological processes (67 % or 20 GO's) with the
640 majority of these occurring at 100 µg/L. When compared to the mixture model at the same
641 concentration, 7 terms are absent in the mixture model compared to the single exposure viz. DNA
642 metabolic processes (GO:0006259), DNA repair (GO:0006281), Cellular response to DNA damage
643 stimulus (GO:0006974), cellular response to stress (GO:0033554), metabolic processes (GO:0008152),
644 cellular metabolic processes (GO:0044237) primary metabolic processes (GO:0044238) and organic

645 substance metabolic processes (GO:0071704). The absence of these enriched terms at the highest
646 mixture concentration of B[a]P and C₆₀ in association with the reduction in differentially expressed
647 proteins (when compared to single exposure and 50 µg/l) suggest an antagonistic interaction between
648 the two common contaminants. This may be explained by known properties of the chemicals. nC₆₀ is
649 an exceptional free radical scavenger [103,104], while B[a]P has been shown to produce free radicals
650 under a variety of conditions [105]. B[a]P contributes approximately 50 % of the total carcinogenic
651 potential of the PAH group [106]. Transcriptomic alterations related to B[a]P are likely to be related
652 to genotoxic mechanisms in addition to other biological processes such as mitochondrial activities
653 and immune response as outlined previously [33]. In contrast, Zhang et al demonstrated that aqueous
654 C₆₀ aggregates induced apoptosis of macrophage by changing the mitochondrial membrane potential
655 [107]. As predicted by the literature, enriched GO terms following single nC₆₀ exposure are
656 predominantly related to changes to the membrane-enclosed, organelle and intracellular lumen,
657 while mixed exposure resulted in enrichment of mitochondrial components (viz. matrix, ribosome
658 and protein complex). This enrichment of organelle cellular components correlates with enrichment
659 of the ribosome KEGG pathway (ko03010, 35 proteins at 1 mg/L C₆₀), suggesting an increase in the
660 production of newly synthesised organelle proteins which must find its way from site of production
661 in the cytosol to the organelle where it functions. It was not feasible to quantify changes in cellular
662 components in the digestive gland during this study however we can postulate from prior studies
663 that observed changes may be linked to changes in the mitochondria. Mitochondria are essential
664 eukaryotic organelles required for a range of metabolic, signalling and development processes. Using
665 fullereneol, a polyhydroxylated fullerene derivative, Yang et al. demonstrated significant changes to
666 isolated mitochondria via mitochondrial swelling, collapse of membrane potential, decreased of
667 membrane fluidity and alterations to the ultrastructure [108]. The increase in protein production via
668 the ribosome at the highest concentration may reflect the activation of a repair mechanism for damage
669 to this structure. In a recent review, the main negative molecular and cellular responses associated
670 with carbon nanotube (CNTs) in mammals were associated with oxidative stress which can promote
671 inflammation, mitochondrial oxidation and activation of apoptosis [109]. Additionally, Zhang et al.
672 reported on a loss in mitochondrial membrane potential in a mouse *in vitro* model, in association with
673 increase in cellular ROS suggesting mitochondria associated apoptosis [107]. In a typical aquatic NPs
674 exposure, uptake is followed by localisation into the endosomes, lysosomes and digestive associated
675 cells as well as the lumen of digestive tubules [22,27,110]. This NP exposure response can be followed
676 by disruption or modification to mitochondrial activity [30]. Although the current study would
677 support the hypothesis of mitochondrial damage/repair, further work will need to be carried out to
678 verify.

679 KEGG pathway analysis can provide physiological pathway information for various
680 experiments with prior studies using it to aid in identification of mode of action of environmental
681 contaminants [68]. In the current study, irrespective of exposure conditions or concentrations, the top
682 enriched pathway identified using KEGG was the Ribosome with 19-39 genes identified in the
683 pathway dependent on treatment and concentration. This was followed by protein processing in the
684 endoplasmic reticulum and carbon metabolism. The ribosome is a large complex molecule made of
685 RNA and proteins that perform the essential task of protein synthesis in the cell. They also serve as
686 the initiation point for several translation-associated functions including protein folding and
687 degradation of defective or nonstop mRNAs. Previous studies have demonstrated a change in
688 regulation of genes which encode ribosomal protein subunits following B[a]P exposure, with the
689 suggestion that mRNA directed protein synthesis is reduced in mussels exposed to higher B[a]P loads
690 [33]. Additionally, *M. Galloprovincialis* has been shown to response to B[a]P exposure via changes in
691 abundance of proteins related to synthesis and degradation, energy supply (via ATP) and structural
692 proteins [68]. Proteomic results for B[a]P exposure to digestive gland tissue are in agreement with
693 prior studies and support the observed trends identified using transcriptomic methodologies. In the
694 second most enriched pathway (viz. protein processing in endoplasmic reticulum), three heat shock
695 proteins viz. *HSP70*, *HSP90* and *HSP40* and other molecular chaperones were identified dependent
696 on exposure conditions. This is not surprising given that many HSPs function as molecular

697 chaperones to protect damaged proteins from aggregation, unfold protein aggregates or refold
698 damaged proteins or target them for efficient removal [111]. These proteins regulate cell response to
699 oxidative stress with HSP70 strongly up-regulated by heat stress and toxic chemicals. HSP70 plays
700 several essential roles in cellular protein metabolism [112,113] while HSP40 facilitates cellular
701 recovery from adverse effects of damaged or misfolded proteins (proteotoxic stress). Changes in
702 HSPs, in addition to up/down regulation of HSP40, HSP70 and HSP90 have typically been reported
703 in response to thermal stress in bivalves [98,114,115] and other environmental contaminants such as
704 B[a]P [33]. In general, the consistent enrichment of genes involved in the Endoplasmic-reticulum
705 associated protein degradation (ERAD) pathway suggest that aqueous fullerene exposure targets the
706 cellular pathway involved in targeting misfolding proteins for ubiquitination (post-translational
707 modification) and subsequent degradation by proteasomes (protein degrading complex, breaks
708 peptide bonds). It is interesting to note the overlap between organismal response to fullerene
709 exposure and that of organismal response to thermal stress. Observed enrichment pathways in the
710 current study viz protein processing in endoplasmic reticulum, apoptosis, ubiquitin mediated
711 proteolysis, endocytosis, spliceosome, and MAPK signalling pathway have been observed as
712 differentially enriched in oysters as a response to thermal stress [114].

713

714

3.4. Notes

715

716

717

718

719

720

721

722

723

724

725

726

727

728

729

730

731

732

733

734

735

736

737

738

739

740

741

742

743

744

745

746

747

748

The lack of consensus regarding C₆₀ toxicity may be partly due limited studies which incorporate both a physiological and ecological approach. As a consequence, little is still known about NP bioavailability, mode of uptake, ingestion rates and actual internal concentrations related to ADME [27]. Generally, the greater the water solubility of fullerene aggregates (through e.g. stirring, surface modifications, sonication), the less the toxicity associated with the exposure [91]. Gomes et al highlights that while mussels represent a target for environmental exposure to nanoparticles, exposure duration may significantly contribute to NPs mediated toxicity [116]. As such, it is possible that the lack of differentially expressed proteins identified in this study is a factor of limited exposure duration. Limited exposure duration in the region of days or hours is common in the literature, and it would be of interest to explore long term exposure to NPs to look at the long term impact and adaptation of mussels in the marine environment. Species specific responses to C₆₀ are abundant in the literature and it would be remiss to not discuss how our results align with other marine invertebrates. Exposure to ROS can cause a range of reversible and irreversible modifications of protein amino acid side-chains which has been reviewed by Ghezzi and Bonetto [117]. Within the field of aquatic ecotoxicology, the toxic impact and potential mechanisms of single contaminant exposures have been extensively studied via laboratory experiments (*in vivo*, *in vitro* and *in silico*) and field monitoring. However, harder to predict is the effects of mixtures of pollutants in the environment. Biological damage observed cannot simply be linked to the actual environmental condition as mixtures of contaminants are known to exist in the aquatic ecosystem. This is further complicated with respect to nanomaterials due to their inherent properties which can amplify or negate the toxic effects of other compounds [69]. Complicated interactions may occur which make interpretation complex. For example, proteomic analysis of *Mytilus galloprovincialis* revealed that single Cu and B[a]P exposure in addition to a combination of the two generate different protein profiles with a non-additive profile [68]. Differences in mixture response compared to single exposure are likely to be related to individual chemical properties and toxicity mechanisms of B[a]P and C₆₀, as has been noted in B[a]P co-exposed with various metals [118]. C₆₀ concentration was kept constant with increasing concentrations of B[a]P in an experimental design that has been previously carried out using algae and crustacean species [22]. This may reflect limited proteome changes at the exposure concentrations, with concentrations of C₆₀ in the range of 10 - 500 ppb have been reported to be 10 fold below the no observable adverse effect level (NOAEL) [119,120]. At 1 mg/L, an increase in GST activity in the digestive gland has been reported [110] C₆₀ is known to bind to minor grooves of double stranded DNA and trigger unwinding and disruption of the DNA helix [102] C₆₀ adsorbs onto cell-membrane P-glycoprotein through hydrophobic interactions, but the stability and secondary structure of the protein are barely affected [121]. P-glycoprotein is present in *Mytilus*

749 *galloprovincialis* [122] C₆₀ and its derivatives are known to impact DNA and RNA in terms of stability,
750 replication and reactivity in addition to structural stabilisation [123,124]. In a recent study, Canesi et
751 al determined that C₆₀ fullerene exposure to *Mytilus galloprovincialis* hemocytes did not induce
752 significant cytotoxicity, and instead stimulated immune and inflammatory parameters such as
753 lysozyme release, oxidative burst and NO production [10]. Nanomaterial suspensions can induce
754 inflammatory processes in bivalve hemocytes akin to those observed in vertebrate cells [10]. Results
755 from mammalian studies suggest that C₆₀ fullerene exposure results predominantly in inflammatory
756 responses [125].

757 5. Conclusions

758 This study has demonstrated for the first time the interaction between two ubiquitous
759 environmental contaminants with an apparent antagonistic relationship at the genotoxic and the
760 proteome expression level. No Trojan horse effects were observed for uptake or toxicity of the co-
761 contaminants B[a]P in interaction with C₆₀. Proteome profile is dependent on concentration and
762 treatment. The exposure to the three conditions had overlap and common mechanisms of response
763 irrespective of differences in mode of action. The provided list of condition specific differentially
764 expressed proteins and enriched pathways (Spreadsheet S1) may represent a step towards
765 definitively identifying mode of action of these compounds in bivalves when combined with other
766 OMICs based approaches. It should be noted that the antagonistic proteome response observed in
767 the current study between B[a]P and C₆₀ is based on a single concentration of the fullerene and as
768 such represents a general overview of toxicological behaviour. It is possible that that this antagonistic
769 interaction will change when another dose range is selected [93]. Gomes et al previously highlighted
770 that while mussels represent a target for environmental exposure to nanoparticles, exposure duration
771 may significantly contribute to NPs mediated toxicity [116]. As such, further work must be carried
772 out to explore mixture effects at different concentrations and over differing exposure duration.

773 **Supplementary Materials:** The following are available online, **Figure S1:** Representative particle size
774 distribution showing the intensity-weighted hydrodynamic diameter (d_H) of nC₆₀ in mussel-exposed
775 seawater as determined by DLS (653±87 nm), **Figure S2:** (a) Bright-field TEM and (b) point EDX
776 spectroscopy analysis of Er₃N@C₈₀, **Figure S3:** Dark-field STEM and EDX spectroscopy mapping
777 analysis of Er₃N@C₈₀, confirming the necessity for spectroscopy to confirm the presence of labelled
778 fullerenes, using the characteristic X-rays emitted from Er upon electron irradiation, **Figure S4:** (a,c,e)
779 Dark-field STEM and (b,d,f) corresponding point EDX spectroscopy analysis of cross-sections of
780 mussel digestive gland exposed to Er₃N@C₈₀, **Table S1:** The influence of benzo(a)pyrene (B[a]P) of the
781 hydrodynamic diameter (d_H) of nC₆₀ in mussel-exposed seawater as determined by DLS, **Table S2:**
782 The concentration of B[a]P in seawater at T0, day 1 and day 3, **Table S3:** The concentration of nC₆₀ in
783 seawater at T0, day 1 and day 3, **Spreadsheet S1:** Full list of DEPs, enriched Gene Ontology (GO)
784 terms and KEGGS pathways, **R script S1:** R script used for proteomics analysis.

785 **Author Contributions:** Conceptualization, A.J.; methodology, A.B., G.R., L.L., V.S., Y.A.; formal analysis, A.B.,
786 L.L., G.R.; investigation, A.B., L.L., G.R., Y.A., N.W., F.A., V.A., V.S.; resources, A.J.; data curation, A.B., L.L., V.S.,
787 G.R.; writing—original draft preparation, A.B., L.L., G.R.; writing—review and editing, A.B., L.L., G.R., Y.A.,
788 N.W., F.A., M.M., V.A., V.S., A.K., J.R., A.J.; visualization, A.B and L.L.; supervision, A.J.; project administration,
789 A.J.; funding acquisition, A.J.

790 **Funding:** This study is mainly supported by Natural Environment Research Council (NERC), UK (Grant No.
791 NE/L006782/1; PI: ANJ). Additional Support from the Engineering and Physical Sciences Research Council
792 (EPSRC) [Grant No. EP/L022494/1] and the University of Nottingham is acknowledged. Work at King's College
793 London was further supported by the National Institute for Health Research Health Protection Research Unit
794 (NIHR HPRU) in Health Impact of Environmental Hazards at King's College London in partnership with Public
795 Health England (PHE) and Imperial College London.

796 **Acknowledgments:**

797 **Conflicts of Interest:** The authors declare no conflict of interest.

798 **References**

- 799 1. Bergin, I.L.; Witzmann, F.A. Nanoparticle toxicity by the gastrointestinal route: evidence and knowledge
800 gaps. *Int. J. Biomed. Nanosci. Nanotechnol.* **2013**, *3*, 163, doi:10.1504/IJBNN.2013.054515.
- 801 2. Cheng, X.; Kan, A.T.; Tomson, M.B. Naphthalene Adsorption and Desorption from Aqueous C60
802 Fullerene. *J. Chem. Eng. Data* **2004**, *49*, 675–683, doi:10.1021/je030247m.
- 803 3. Georgakilas, V.; Perman, J.A.; Tucek, J.; Zboril, R. Broad Family of Carbon Nanoallotropes:
804 Classification, Chemistry, and Applications of Fullerenes, Carbon Dots, Nanotubes, Graphene,
805 Nanodiamonds, and Combined Superstructures. *Chem. Rev.* **2015**, *115*, 4744–4822, doi:10.1021/cr500304f.
- 806 4. Andrievsky, G.; Klochkov, V.; Karyakina, E.; Mchedlov-Petrosyan, N.. Studies of aqueous colloidal
807 solutions of fullerene C60 by electron microscopy. *Chem. Phys. Lett.* **1999**, *300*, 392–396,
808 doi:10.1016/S0009-2614(98)01393-1.
- 809 5. Chen, Z.; Westerhoff, P.; Herckes, P. Quantification of C60 fullerene concentrations in water. *Environ.*
810 *Toxicol. Chem.* **2008**, *27*, 1852, doi:10.1897/07-560.1.
- 811 6. Henry, T.B.; Petersen, E.J.; Compton, R.N. Aqueous fullerene aggregates (nC60) generate minimal
812 reactive oxygen species and are of low toxicity in fish: A revision of previous reports. *Curr. Opin.*
813 *Biotechnol.* **2011**, *22*, 533–537, doi:10.1016/j.copbio.2011.05.511.
- 814 7. Markovic, Z.; Trajkovic, V. Biomedical potential of the reactive oxygen species generation and
815 quenching by fullerenes (C60). *Biomaterials* **2008**, *29*, 3561–3573, doi:10.1016/j.biomaterials.2008.05.005.
- 816 8. Blickley, T.M.; McClellan-Green, P. TOXICITY OF AQUEOUS FULLERENE IN ADULT AND LARVAL
817 FUNDULUS HETEROCLITUS. *Environ. Toxicol. Chem.* **2008**, *27*, 1964, doi:10.1897/07-632.1.
- 818 9. Della Torre, C.; Maggioni, D.; Ghilardi, A.; Parolini, M.; Santo, N.; Landi, C.; Madaschi, L.; Magni, S.;
819 Tasselli, S.; Ascagni, M.; et al. The interactions of fullerene C60 and Benzo(A)pyrene influence their
820 bioavailability and toxicity to zebrafish embryos. *Environ. Pollut.* **2018**, *241*, 999–1008,
821 doi:10.1016/j.envpol.2018.06.042.
- 822 10. Canesi, L.; Ciacci, C.; Vallotto, D.; Gallo, G.; Marcomini, A.; Pojana, G. In vitro effects of suspensions of
823 selected nanoparticles (C60 fullerene, TiO2, SiO2) on *Mytilus* hemocytes. *Aquat. Toxicol.* **2010**, *96*, 151–
824 158, doi:10.1016/j.aquatox.2009.10.017.
- 825 11. Freixa, A.; Acuña, V.; Gutierrez, M.; Sanchís, J.; Santos, L.H.M.L.M.; Rodriguez-Mozaz, S.; Farré, M.;
826 Barceló, D.; Sabater, S. Fullerenes influence the toxicity of organic micro-contaminants to river biofilms.
827 *Front. Microbiol.* **2018**, *9*, 1–12, doi:10.3389/fmicb.2018.01426.
- 828 12. Yang, J.L.; Li, Y.F.; Guo, X.P.; Liang, X.; Xu, Y.F.; Ding, D.W.; Bao, W.Y.; Dobretsov, S. The effect of carbon
829 nanotubes and titanium dioxide incorporated in PDMS on biofilm community composition and
830 subsequent mussel plantigrade settlement. *Biofouling* **2016**, *32*, 763–777,
831 doi:10.1080/08927014.2016.1197210.

- 832 13. Lehto, M.; Karilainen, T.; Róg, T.; Cramariuc, O.; Vanhala, E.; Tornaueus, J.; Taberman, H.; Jänis, J.;
833 Alenius, H.; Vattulainen, I.; et al. Co-Exposure with Fullerene May Strengthen Health Effects of Organic
834 Industrial Chemicals. *PLoS One* **2014**, *9*, e114490, doi:10.1371/journal.pone.0114490.
- 835 14. Park, J.-W.; Henry, T.B.; Ard, S.; Menn, F.-M.; Compton, R.N.; Sayler, G.S. The association between
836 nC(60) and 17 α -ethinylestradiol (EE2) decreases EE2 bioavailability in zebrafish and alters
837 nanoaggregate characteristics. *Nanotoxicology* **2011**, *5*, 406–416, doi:10.3109/17435390.2010.525329.
- 838 15. Kim, K.T.; Jang, M.H.; Kim, J.Y.; Kim, S.D. Effect of preparation methods on toxicity of fullerene water
839 suspensions to Japanese medaka embryos. *Sci. Total Environ.* **2010**, *408*, 5606–5612,
840 doi:10.1016/j.scitotenv.2010.07.055.
- 841 16. Nielsen, G.D.; Roursgaard, M.; Jensen, K.A.; Poulsen, S.S.; Larsen, S.T. In vivo biology and toxicology of
842 fullerenes and their derivatives. *Basic Clin. Pharmacol. Toxicol.* **2008**, *103*, 197–208, doi:10.1111/j.1742-
843 7843.2008.00266.x.
- 844 17. Fiorito, S.; Serafino, A.; Andreola, F.; Bernier, P. Effects of fullerenes and single-wall carbon nanotubes
845 on murine and human macrophages. *Carbon N. Y.* **2006**, *44*, 1100–1105, doi:10.1016/j.carbon.2005.11.009.
- 846 18. Oberdörster, G.; Oberdörster, E.; Oberdörster, J. Nanotoxicology: an emerging discipline evolving from
847 studies of ultrafine particles. *Environ. Health Perspect.* **2005**, *113*, 823–39, doi:10.1289/ehp.7339.
- 848 19. Kennedy, A.J.; Hull, M.S.; Steevens, J.A.; Dontsova, K.M.; Chappell, M.A.; Gunter, J.C.; Weiss, C.A.
849 Factors influencing the partitioning and toxicity of nanotubes in the aquatic environment. *Environ.*
850 *Toxicol. Chem.* **2008**, *27*, 1932–1941, doi:10.1897/07-624.1.
- 851 20. Trpkovic, A.; Todorovic-Markovic, B.; Trajkovic, V. Toxicity of pristine versus functionalized fullerenes:
852 Mechanisms of cell damage and the role of oxidative stress. *Arch. Toxicol.* **2012**, *86*, 1809–1827,
853 doi:10.1007/s00204-012-0859-6.
- 854 21. Zhu, S.; Oberdörster, E.; Haasch, M.L. Toxicity of an engineered nanoparticle (fullerene, C60) in two
855 aquatic species, *Daphnia* and fathead minnow. *Mar. Environ. Res.* **2006**, *62*, S5,
856 doi:10.1016/j.marenvres.2006.04.059.
- 857 22. Baun, A.; Sørensen, S.N.; Rasmussen, R.F.; Hartmann, N.B.; Koch, C.B. Toxicity and bioaccumulation of
858 xenobiotic organic compounds in the presence of aqueous suspensions of aggregates of nano-C60. *Aquat.*
859 *Toxicol.* **2008**, *86*, 379–387, doi:10.1016/j.aquatox.2007.11.019.
- 860 23. Henry, T.B.; Wileman, S.J.; Boran, H.; Sutton, P. Association of Hg 2+ with Aqueous (C 60) n Aggregates
861 Facilitates Increased Bioavailability of Hg 2+ in Zebrafish (*Danio rerio*). *Environ. Sci. Technol.* **2013**, *47*,
862 9997–10004, doi:10.1021/es4015597.
- 863 24. Velzeboer, I.; Kwadijk, C.J.A.F.; Koelmans, A.A. Strong Sorption of PCBs to Nanoplastics, Microplastics,
864 Carbon Nanotubes, and Fullerenes. *Environ. Sci. Technol.* **2014**, *48*, 4869–4876, doi:10.1021/es405721v.
- 865 25. Farkas, J.; Bergum, S.; Nilsen, E.W.; Olsen, A.J.; Salaberria, I.; Ciesielski, T.M.; Baczek, T.; Konieczna, L.;
866 Salvenmoser, W.; Jenssen, B.M. The impact of TiO₂ nanoparticles on uptake and toxicity of

- 867 benzo(a)pyrene in the blue mussel (*Mytilus edulis*). *Sci. Total Environ.* **2015**, *511*, 469–476,
868 doi:10.1016/j.scitotenv.2014.12.084.
- 869 26. Holmstrup, M.; Bindesbøl, A.M.; Oostingh, G.J.; Duschl, A.; Scheil, V.; Köhler, H.R.; Loureiro, S.; Soares,
870 A.M.V.M.; Ferreira, A.L.G.; Kienle, C.; et al. Interactions between effects of environmental chemicals and
871 natural stressors: A review. *Sci. Total Environ.* **2010**, *408*, 3746–3762, doi:10.1016/j.scitotenv.2009.10.067.
- 872 27. Canesi, L.; Ciacci, C.; Fabbri, R.; Marcomini, A.; Pojana, G.; Gallo, G. Bivalve molluscs as a unique target
873 group for nanoparticle toxicity. *Mar. Environ. Res.* **2012**, *76*, 16–21, doi:10.1016/j.marenvres.2011.06.005.
- 874 28. de Lafontaine, Y.; Gagné, F.; Blaise, C.; Costan, G.; Gagnon, P.; Chan, H.M. Biomarkers in zebra mussels
875 (*Dreissena polymorpha*) for the assessment and monitoring of water quality of the St Lawrence River
876 (Canada). *Aquat. Toxicol.* **2000**, *50*, 51–71, doi:10.1016/S0166-445X(99)00094-6.
- 877 29. Hu, M.; Lin, D.; Shang, Y.; Hu, Y.; Lu, W.; Huang, X.; Ning, K.; Chen, Y.; Wang, Y. CO₂-induced pH
878 reduction increases physiological toxicity of nano-TiO₂ in the mussel *Mytilus coruscus*. *Sci. Rep.* **2017**,
879 *7*, 1–11, doi:10.1038/srep40015.
- 880 30. Gomes, T.; Pereira, C.G.; Cardoso, C.; Bebianno, M.J. Differential protein expression in mussels *Mytilus*
881 *galloprovincialis* exposed to nano and ionic Ag. *Aquat. Toxicol.* **2013**, *136–137*, 79–90,
882 doi:10.1016/j.aquatox.2013.03.021.
- 883 31. D’Agata, A.; Fasulo, S.; Dallas, L.J.; Fisher, A.S.; Maisano, M.; Readman, J.W.; Jha, A.N. Enhanced toxicity
884 of “bulk” titanium dioxide compared to “fresh” and “aged” nano-TiO₂ in marine mussels (*Mytilus*
885 *galloprovincialis*). *Nanotoxicology* **2014**, *8*, 549–58, doi:10.3109/17435390.2013.807446.
- 886 32. Dallas, L.J.; Bean, T.P.; Turner, A.; Lyons, B.P.; Jha, A.N. Oxidative DNA damage may not mediate Ni-
887 induced genotoxicity in marine mussels: assessment of genotoxic biomarkers and transcriptional
888 responses of key stress genes. *Mutat. Res.* **2013**, *754*, 22–31, doi:10.1016/j.mrgentox.2013.03.009.
- 889 33. Banni, M.; Sforzini, S.; Arlt, V.M.; Barranger, A.; Dallas, L.J.; Oliveri, C.; Aminot, Y.; Pacchioni, B.;
890 Millino, C.; Lanfranchi, G.; et al. Assessing the impact of Benzo[a]pyrene on Marine Mussels:
891 Application of a novel targeted low density microarray complementing classical biomarker responses.
892 *PLoS One* **2017**, *12*, e0178460, doi:10.1371/journal.pone.0178460.
- 893 34. Sanchís, J.; Aminot, Y.; Abad, E.; Jha, A.N.; Readman, J.W.; Farré, M. Transformation of C60 fullerene
894 aggregates suspended and weathered under realistic environmental conditions. *Carbon N. Y.* **2018**, *128*,
895 54–62, doi:10.1016/j.carbon.2017.11.060.
- 896 35. Wiśniewski, J.R.; Zougman, A.; Nagaraj, N.; Mann, M. Universal sample preparation method for
897 proteome analysis. *Nat. Methods* **2009**, *6*, 359, Universal sample preparation method for proteome
898 analysis. *Nat. Methods* **2009**, *6*, 359.
- 899 36. Rappsilber, J.; Ishihama, Y.; Mann, M. Stop and Go Extraction Tips for Matrix-Assisted Laser
900 Desorption/Ionization, Nanoelectrospray, and LC/MS Sample Pretreatment in Proteomics. *Anal. Chem.*
901 **2003**, *75*, 663–670, doi:10.1021/ac026117i.

- 902 37. Sequiera, G.L.; Sareen, N.; Sharma, V.; Surendran, A.; Abu-El-Rub, E.; Ravandi, A.; Dhingra, S. High
903 throughput screening reveals no significant changes in protein synthesis, processing, and degradation
904 machinery during passaging of mesenchymal stem cells. *Can. J. Physiol. Pharmacol.* **2018**, *1–8*,
905 doi:10.1139/cjpp-2018-0553.
- 906 38. R Development Core Team. R: A Language and Environment for Statistical Computing 2013.
- 907 39. Kessner, D.; Chambers, M.; Burke, R.; Agus, D.; Mallick, P. ProteoWizard: Open source software for
908 rapid proteomics tools development. *Bioinformatics* **2008**, *24*, 2534–2536,
909 doi:10.1093/bioinformatics/btn323.
- 910 40. Pedersen, T.L. MSGFplus: An interface between R and MS-GF+ 2017.
- 911 41. Kim, S.; Pevzner, P.A. MS-GF+ makes progress towards a universal database search tool for proteomics.
912 *Nat. Commun.* **2014**, *5*, 1–10, doi:10.1038/ncomms6277.
- 913 42. Ding, Q.; Zhang, J. seqRFLP: Simulation and visualization of restriction enzyme cutting pattern from
914 DNA sequences 2012.
- 915 43. Levitsky, L.I.; Ivanov, M. V; Lobas, A.A.; Gorshkov, M. V Unbiased False Discovery Rate Estimation for
916 Shotgun Proteomics Based on the Target-Decoy Approach. *J. Proteome Res.* **2017**, *16*, 393–397,
917 doi:10.1021/acs.jproteome.6b00144.
- 918 44. Deutsch, E.W.; Csordas, A.; Sun, Z.; Jarnuczak, A.; Perez-Riverol, Y.; Ternent, T.; Campbell, D.S.; Bernal-
919 Llinares, M.; Okuda, S.; Kawano, S.; et al. The ProteomeXchange consortium in 2017: supporting the
920 cultural change in proteomics public data deposition. *Nucleic Acids Res.* **2017**, *45*, D1100–D1106,
921 doi:10.1093/nar/gkw936.
- 922 45. Perez-Riverol, Y.; Csordas, A.; Bai, J.; Bernal-Llinares, M.; Hewapathirana, S.; Kundu, D.J.; Inuganti, A.;
923 Griss, J.; Mayer, G.; Eisenacher, M.; et al. The PRIDE database and related tools and resources in 2019:
924 improving support for quantification data. *Nucleic Acids Res.* **2019**, *47*, D442–D450,
925 doi:10.1093/nar/gky1106.
- 926 46. Fu, X.; Gharib, S.A.; Green, P.S.; Aitken, M.L.; Frazer, D.A.; Park, D.R.; Vaisar, T.; Heinecke, J.W. Spectral
927 index for assessment of differential protein expression in shotgun proteomics. *J. Proteome Res.* **2008**, *7*,
928 845–54, doi:10.1021/pr070271+.
- 929 47. Pursiheimo, A.; Vehmas, A.P.; Afzal, S.; Suomi, T.; Chand, T.; Strauss, L.; Poutanen, M.; Rokka, A.;
930 Corthals, G.L.; Elo, L.L. Optimization of Statistical Methods Impact on Quantitative Proteomics Data. *J.*
931 *Proteome Res.* **2015**, *14*, 4118–4126, doi:10.1021/acs.jproteome.5b00183.
- 932 48. Karpievitch, Y. V.; Dabney, A.R.; Smith, R.D. Normalization and missing value imputation for label-free
933 LC-MS analysis. *BMC Bioinformatics* **2012**, *13 Suppl 1*, doi:10.1186/1471-2105-13-S16-S5.
- 934 49. Välikangas, T.; Suomi, T.; Elo, L.L. A systematic evaluation of normalization methods in quantitative
935 label-free proteomics. *Brief. Bioinform.* **2018**, *19*, 1–11, doi:10.1093/bib/bbw095.

- 936 50. Wei, R.; Wang, J.; Su, M.; Jia, E.; Chen, S.; Chen, T.; Ni, Y. Missing Value Imputation Approach for Mass
937 Spectrometry-based Metabolomics Data. *Sci. Rep.* **2018**, *8*, 663, doi:10.1038/s41598-017-19120-0.
- 938 51. Lazar, C.; Gatto, L.; Ferro, M.; Bruley, C.; Burger, T. Accounting for the Multiple Natures of Missing
939 Values in Label-Free Quantitative Proteomics Data Sets to Compare Imputation Strategies. *J. Proteome*
940 *Res.* **2016**, *15*, 1116–1125, doi:10.1021/acs.jproteome.5b00981.
- 941 52. Gregori, J.; Sanchez, A.; Villanueva, J. msmsEDA and msmsTests : R / Bioconductor packages for spectral
942 count label-free proteomics data analysis msmsEDA and msmsTests : R / Bioconductor packages for
943 spectral count label-free proteomics data analysis 2016.
- 944 53. Yu, G.; Wang, L.-G.; Han, Y.; He, Q.-Y. clusterProfiler: an R Package for Comparing Biological Themes
945 Among Gene Clusters. *Omi. A J. Integr. Biol.* **2012**, *16*, 284–287, doi:10.1089/omi.2011.0118.
- 946 54. Kanehisa, M.; Sato, Y.; Morishima, K. BlastKOALA and GhostKOALA: KEGG Tools for Functional
947 Characterization of Genome and Metagenome Sequences. *J. Mol. Biol.* **2016**, *428*, 726–731,
948 doi:10.1016/j.jmb.2015.11.006.
- 949 55. Oliveros, J. VENNY. An interactive tool for comparing lists with Venn's diagrams 2007.
- 950 56. Helbock, H.J.; Beckman, K.B.; Shigenaga, M.K.; Walter, P.B.; Woodall, a a; Yeo, H.C.; Ames, B.N. DNA
951 oxidation matters: the HPLC-electrochemical detection assay of 8-oxo-deoxyguanosine and 8-oxo-
952 guanine. *Proc. Natl. Acad. Sci. U. S. A.* **1998**, *95*, 288–293, doi:10.1073/pnas.95.1.288.
- 953 57. Akcha, F.; Burgeot, T.; Budzinski, H.; Pfohl-Leszkowicz, a; Narbonne, J. Induction and elimination of
954 bulky benzo[a]pyrene-related DNA adducts and 8-oxodGuo in mussels *Mytilus galloprovincialis*
955 exposed in vivo to B[a]P-contaminated feed. *Mar. Ecol. Prog. Ser.* **2000**, *205*, 195–206,
956 doi:10.3354/meps205195.
- 957 58. Barranger, A.; Heude-Berthelin, C.; Rouxel, J.; Adeline, B.; Benabdelmouna, A.; Burgeot, T.; Akcha, F.
958 Parental exposure to the herbicide diuron results in oxidative DNA damage to germinal cells of the
959 Pacific oyster *Crassostrea gigas*. *Comp. Biochem. Physiol. Part - C Toxicol. Pharmacol.* **2016**, *180*, 23–30,
960 doi:10.1016/j.cbpc.2015.11.002.
- 961 59. Phillips, D.H.; Arlt, V.M. 32P-Postlabeling Analysis of DNA Adducts. In *Molecular Toxicology Protocols*;
962 Keohavong, P., Grant, S.G., Eds.; Humana Press: Totowa, NJ, 2014; pp. 127–138 ISBN 978-1-62703-739-6.
- 963 60. Reed, L.; Mrizova, I.; Barta, F.; Indra, R.; Moserova, M.; Kopka, K.; Schmeiser, H.H.; Wolf, C.R.;
964 Henderson, C.J.; Stiborova, M.; et al. Cytochrome b5 impacts on cytochrome P450-mediated metabolism
965 of benzo[a]pyrene and its DNA adduct formation: studies in hepatic cytochrome b5/P450 reductase null
966 (HBRN) mice. *Arch. Toxicol.* **2018**, *92*, 1625–1638, doi:10.1007/s00204-018-2162-7.
- 967 61. Kucab, J.E.; van Steeg, H.; Luijten, M.; Schmeiser, H.H.; White, P.A.; Phillips, D.H.; Arlt, V.M. TP53
968 mutations induced by BPDE in Xpa-WT and Xpa-Null human TP53 knock-in (Hupki) mouse embryo
969 fibroblasts. *Mutat. Res. - Fundam. Mol. Mech. Mutagen.* **2015**, *773*, 48–62,
970 doi:10.1016/j.mrfmmm.2015.01.013.

- 971 62. R Core Team (2019). R: A language and environment for statistical computing. R Foundation for
972 Statistical Computing, Vienna, Austria. URL <https://www.R-project.org/>.
- 973 63. David, R.; Ebbels, T.; Gooderham, N. Synergistic and Antagonistic Mutation Responses of Human MCL-
974 5 Cells to Mixtures of Benzo[a]pyrene and 2-Amino-1-Methyl-6-Phenylimidazo[4,5- b]pyridine: Dose-
975 Related Variation in the Joint Effects of Common Dietary Carcinogens. *Environ. Health Perspect.* **2016**,
976 *124*, 88–96, doi:10.1289/ehp.1409557.
- 977 64. Katsifis, S.P.; Kinney, P.L.; Hosselet, S.; Burns, F.J.; Christie, N.T. Interaction of nickel with mutagens in
978 the induction of sister chromatid exchanges in human lymphocytes. *Mutat. Res. Mutagen. Relat. Subj.*
979 **1996**, *359*, 7–15, doi:10.1016/S0165-1161(96)90004-7.
- 980 65. Schlesinger, R.B.; Zelikoff, J.T.; Chen, L.C.; Kinney, P.L. Assessment of toxicologic interactions resulting
981 from acute inhalation exposure to sulfuric acid and ozone mixtures. *Toxicol. Appl. Pharmacol.* **1992**, *115*,
982 183–190, doi:10.1016/0041-008X(92)90322-J.
- 983 66. Murgarella, M.; Puiu, D.; Novoa, B.; Figueras, A.; Posada, D.; Canchaya, C. A first insight into the
984 genome of the filter-feeder mussel *Mytilus galloprovincialis*. *PLoS One* **2016**, *11*, 1–22,
985 doi:10.1371/journal.pone.0160081.
- 986 67. Song, Q.; Chen, H.; Li, Y.; Zhou, H.; Han, Q.; Diao, X. Toxicological effects of benzo(a)pyrene, DDT and
987 their mixture on the green mussel *Perna viridis* revealed by proteomic and metabolomic approaches.
988 *Chemosphere* **2016**, *144*, 214–224, doi:10.1016/j.chemosphere.2015.08.029.
- 989 68. Maria, V.L.; Gomes, T.; Barreira, L.; Bebianno, M.J. Impact of benzo(a)pyrene, Cu and their mixture on
990 the proteomic response of *Mytilus galloprovincialis*. *Aquat. Toxicol.* **2013**, *144–145*, 284–295,
991 doi:10.1016/j.aquatox.2013.10.009.
- 992 69. Ferreira, J.L.R.; Lonné, M.N.; França, T.A.; Maximilla, N.R.; Lugokenski, T.H.; Costa, P.G.; Fillmann, G.;
993 Antunes Soares, F.A.; de la Torre, F.R.; Monserrat, J.M. Co-exposure of the organic nanomaterial
994 fullerene C60 with benzo[a]pyrene in *Danio rerio* (zebrafish) hepatocytes: Evidence of toxicological
995 interactions. *Aquat. Toxicol.* **2014**, *147*, 76–83, doi:10.1016/j.aquatox.2013.12.007.
- 996 70. Yan, X.M.; Zha, J.M.; Shi, B.Y.; Wang, D.S.; Wang, Z.J.; Tang, H.X. In vivo toxicity of nano-C60 aggregates
997 complex with atrazine to aquatic organisms. *Chinese Sci. Bull.* **2010**, *55*, 339–345, doi:10.1007/s11434-009-
998 0702-5.
- 999 71. Fitzpatrick, P.J.; Krag, T.O.B.; Højrup, P.; Sheehan, D. Characterization of a glutathione S -transferase
1000 and a related glutathione-binding protein from gill of the blue mussel, *Mytilus edulis* . *Biochem. J.* **2015**,
1001 *305*, 145–150, doi:10.1042/bj3050145.
- 1002 72. Di, Y.; Aminot, Y.; Schroeder, D.C.; Readman, J.W.; Jha, A.N. Integrated biological responses and tissue-
1003 specific expression of p53 and ras genes in marine mussels following exposure to benzo(α)pyrene and
1004 C60 fullerenes, either alone or in combination. *Mutagenesis* **2016**, *00*, 1–14, doi:10.1093/mutage/gew049.
- 1005 73. Gomes, T.; Pereira, C.G.; Cardoso, C.; Sousa, V.S.; Teixeira, M.R.; Pinheiro, J.P.; Bebianno, M.J. Effects of

- 1006 silver nanoparticles exposure in the mussel *Mytilus galloprovincialis*. *Mar. Environ. Res.* **2014**, *101*, 208–
1007 214, doi:10.1016/j.marenvres.2014.07.004.
- 1008 74. Tedesco, S.; Doyle, H.; Redmond, G.; Sheehan, D. Gold nanoparticles and oxidative stress in *Mytilus*
1009 *edulis*. *Mar. Environ. Res.* **2008**, *66*, 131–133, doi:10.1016/j.marenvres.2008.02.044.
- 1010 75. Kahru, A.; Dubourguier, H.C. From ecotoxicology to nanoecotoxicology. *Toxicology* **2010**, *269*, 105–119,
1011 doi:10.1016/j.tox.2009.08.016.
- 1012 76. Isakovic, A.; Markovic, Z.; Todorovic-Marcovic, B.; Nikolic, N.; Vranjes-Djuric, S.; Mirkovic, M.;
1013 Dramicanin, M.; Harhaji, L.; Raicevic, N.; Nikolic, Z.; et al. Distinct cytotoxic mechanisms of pristine
1014 versus hydroxylated fullerene. *Toxicol. Sci.* **2006**, *91*, 173–183, doi:10.1093/toxsci/kfj127.
- 1015 77. Du, C.; Zhang, B.; He, Y.; Hu, C.; Ng, Q.X.; Zhang, H.; Ong, C.N.; ZhifenLin Biological effect of aqueous
1016 C60 aggregates on *Scenedesmus obliquus* revealed by transcriptomics and non-targeted metabolomics.
1017 *J. Hazard. Mater.* **2017**, *324*, 221–229, doi:10.1016/j.jhazmat.2016.10.052.
- 1018 78. Kuznetsova, G.P.; Larina, O. V.; Petushkova, N.A.; Kisrieva, Y.S.; Samenkova, N.F.; Trifonova, O.P.;
1019 Karuzina, I.I.; Ipatova, O.M.; Zolotaryov, K. V.; Romashova, Y.A.; et al. Effects of fullerene C60 on
1020 proteomic profile of danio rerio fish embryos. *Bull. Exp. Biol. Med.* **2014**, *156*, 694–698, doi:10.1007/s10517-
1021 014-2427-y.
- 1022 79. Levi, N.; Hantgan, R.R.; Lively, M.O.; Carroll, D.L.; Prasad, G.L. C60-Fullerenes: Detection of
1023 intracellular photoluminescence and lack of cytotoxic effects. *J. Nanobiotechnology* **2006**, *4*, 1–11,
1024 doi:10.1186/1477-3155-4-14.
- 1025 80. Hüffer, T.; Kah, M.; Hofmann, T.; Schmidt, T.C. How redox conditions and irradiation affect sorption of
1026 PAHs by dispersed fullerenes (nC60). *Environ. Sci. Technol.* **2013**, *47*, 6935–6942, doi:10.1021/es303620c.
- 1027 81. Linard, E.N.; Apul, O.G.; Karanfil, T.; Van Den Hurk, P.; Klaine, S.J. Bioavailability of Carbon
1028 Nanomaterial-Adsorbed Polycyclic Aromatic Hydrocarbons to Pimphales promelas: Influence of
1029 Adsorbate Molecular Size and Configuration. *Environ. Sci. Technol.* **2017**, *51*, 9288–9296,
1030 doi:10.1021/acs.est.7b02164.
- 1031 82. Santín, G.; Eljarrat, E.; Barceló, D. Bioavailability of classical and novel flame retardants: Effect of
1032 fullerene presence. *Sci. Total Environ.* **2016**, *565*, 299–305, doi:10.1016/j.scitotenv.2016.04.155.
- 1033 83. Sanchís, J.; Olmos, M.; Vincent, P.; Farré, M.; Barceló, D. New Insights on the Influence of Organic Co-
1034 Contaminants on the Aquatic Toxicology of Carbon Nanomaterials. *Environ. Sci. Technol.* **2016**, *50*, 961–
1035 969, doi:10.1021/acs.est.5b03966.
- 1036 84. Su, Y.; Yan, X.; Pu, Y.; Xiao, F.; Wang, D.; Yang, M. Risks of single-walled carbon nanotubes acting as
1037 contaminants-carriers: Potential release of phenanthrene in Japanese medaka (*Oryzias latipes*). *Environ.*
1038 *Sci. Technol.* **2013**, *47*, 4704–4710, doi:10.1021/es304479w.
- 1039 85. Della Torre, C.; Parolini, M.; Del Giacco, L.; Ghilardi, A.; Ascagni, M.; Santo, N.; Maggioni, D.; Magni,
1040 S.; Madaschi, L.; Prospero, L.; et al. Adsorption of B(α)P on carbon nanopowder affects accumulation and

- 1041 toxicity in zebrafish (*Danio rerio*) embryos. *Environ. Sci. Nano* **2017**, *4*, doi:10.1039/c7en00154a.
- 1042 86. Xia, X.; Chen, X.; Zhao, X.; Chen, H.; Shen, M. Effects of carbon nanotubes, chars, and ash on
1043 bioaccumulation of perfluorochemicals by *Chironomus plumosus* larvae in sediment. *Environ. Sci.*
1044 *Technol.* **2012**, *46*, 12467–12475, doi:10.1021/es303024x.
- 1045 87. Al-Subiai, S.N.; Arlt, V.M.; Frickers, P.E.; Readman, J.W.; Stolpe, B.; Lead, J.R.; Moody, A.J.; Jha, A.N.
1046 Merging nano-genotoxicology with eco-genotoxicology: An integrated approach to determine
1047 interactive genotoxic and sub-lethal toxic effects of C 60 fullerenes and fluoranthene in marine mussels,
1048 *Mytilus* sp. *Mutat. Res. - Genet. Toxicol. Environ. Mutagen.* **2012**, *745*, 92–103,
1049 doi:10.1016/j.mrgentox.2011.12.019.
- 1050 88. Sanchís, J.; Llorca, M.; Olmos, M.; Schirinzi, G.F.; Bosch-Orea, C.; Abad, E.; Barceló, D.; Farré, M.
1051 Metabolic Responses of *Mytilus galloprovincialis* to Fullerenes in Mesocosm Exposure Experiments.
1052 *Environ. Sci. Technol.* **2018**, *52*, 1002–1013, doi:10.1021/acs.est.7b04089.
- 1053 89. Brunk, U.T.; Terman, A. Lipofuscin: Mechanisms of age-related accumulation and influence on cell
1054 function. *Free Radic. Biol. Med.* **2002**, *33*, 611–619, doi:10.1016/S0891-5849(02)00959-0.
- 1055 90. Sforzini, S.; Moore, M.N.; Oliveri, C.; Volta, A.; Jha, A.; Banni, M.; Viarengo, A. Role of mTOR in
1056 autophagic and lysosomal reactions to environmental stressors in molluscs. *Aquat. Toxicol.* **2018**, *195*,
1057 114–128, doi:10.1016/j.aquatox.2017.12.014.
- 1058 91. Johnston, H.J.; Hutchison, G.R.; Christensen, F.M.; Aschberger, K.; Stone, V. The biological mechanisms
1059 and physicochemical characteristics responsible for driving fullerene toxicity. *Toxicol. Sci.* **2009**, *114*, 162–
1060 182, doi:10.1093/toxsci/kfp265.
- 1061 92. Rondags, A.; Yuen, W.Y.; Jonkman, M.F.; Horváth, B. Fullerene C60 with cytoprotective and cytotoxic
1062 potential: prospects as a novel treatment agent in Dermatology? *Exp. Dermatol.* **2017**, *26*, 220–224,
1063 doi:10.1111/exd.13172.
- 1064 93. Groten, J.P.; Feron, V.J.; Suhnel, J. Toxicology of simple and complex mixtures. *Trends Pharmacol. Sci.*
1065 **2001**, *22*, 316–322, Toxicology of simple and complex mixtures. *Trends Pharmacol. Sci.* 2001, 22, 316–322.
- 1066 94. Slattery, M.; Ankisetty, S.; Corrales, J.; Marsh-Hunkin, K.E.; Gochfeld, D.J.; Willett, K.L.; Rimoldi, J.M.
1067 Marine proteomics: A critical assessment of an emerging technology. *J. Nat. Prod.* **2012**, *75*, 1833–1837,
1068 doi:10.1021/np300366a.
- 1069 95. Campos, A.; Danielsson, G.; Farinha, A.P.; Kuruvilla, J.; Warholm, P.; Cristobal, S. Shotgun proteomics
1070 to unravel marine mussel (*Mytilus edulis*) response to long-term exposure to low salinity and
1071 propranolol in a Baltic Sea microcosm. *J. Proteomics* **2016**, *137*, 97–106, doi:10.1016/j.jprot.2016.01.010.
- 1072 96. Pales Espinosa, E.; Koller, A.; Allam, B. Proteomic characterization of mucosal secretions in the eastern
1073 oyster, *Crassostrea virginica*. *J. Proteomics* **2016**, *132*, 63–76, doi:10.1016/j.jprot.2015.11.018.
- 1074 97. Campos, A.; Apraiz, I.; da Fonseca, R.R.; Cristobal, S. Shotgun analysis of the marine mussel *Mytilus*
1075 *edulis* hemolymph proteome and mapping the innate immunity elements. *Proteomics* **2015**, *15*, 4021–

- 1076 4029, doi:10.1002/pmic.201500118.
- 1077 98. Fields, P.A.; Zuzow, M.J.; Tomanek, L. Proteomic responses of blue mussel (*Mytilus*) congeners to
1078 temperature acclimation. *J. Exp. Biol.* **2012**, *215*, 1106–1116, doi:10.1242/jeb.062273.
- 1079 99. Franco-Martínez, L.; Martínez-Subiela, S.; Escribano, D.; Schlosser, S.; Nöbauer, K.; Razzazi-Fazeli, E.;
1080 Romero, D.; Cerón, J.J.; Tvarijonavičiute, A. Alterations in haemolymph proteome of *Mytilus*
1081 *galloprovincialis* mussel after an induced injury. *Fish Shellfish Immunol.* **2018**, *75*, 41–47,
1082 doi:10.1016/j.fsi.2018.01.038.
- 1083 100. De Rosa, C.T.; El-Masri, H.A.; Pohl, H.; Cibulas, W.; Mumtaz, M.M. IMPLICATIONS OF CHEMICAL
1084 MIXTURES IN PUBLIC HEALTH PRACTICE. *J. Toxicol. Environ. Heal. Part B* **2004**, *7*, 339–350,
1085 doi:10.1080/10937400490498075.
- 1086 101. Rey-Salgueiro, L.; Martínez-Carballo, E.; Cid, A.; Simal-Gándara, J. Determination of kinetic
1087 bioconcentration in mussels after short term exposure to polycyclic aromatic hydrocarbons. *Heliyon*
1088 **2017**, *3*, e00231, doi:10.1016/j.heliyon.2017.e00231.
- 1089 102. Xu, J.; Corry, D.; Patton, D.; Liu, J.; Jackson, S. F-Actin Plaque Formation as a Transitional Membrane
1090 Microstructure Which Plays a Crucial Role in Cell-cell Reconnections of Rat Hepatic Cells After Isolation.
1091 *J. Interdiscip. Histopathol.* **2012**, *1*, 50, doi:10.5455/jihp.20121209033242.
- 1092 103. Anilkumar, P.; Lu, F.; Cao, L.; G. Luo, P.; Liu, J.-H.; Sahu, S.; N. Tackett II, K.; Wang, Y.; Sun, Y.-P.
1093 Fullerenes for Applications in Biology and Medicine. *Curr. Med. Chem.* **2011**, *18*, 2045–2059,
1094 doi:10.2174/092986711795656225.
- 1095 104. Bakry, R.; Vallant, R.M.; Najam-ul-Haq, M.; Rainer, M.; Szabo, Z.; Huck, C.W.; Bonn, G.K. Medicinal
1096 applications of fullerenes. *Int. J. Nanomedicine* **2007**, *2*, 639–649, Medicinal applications of fullerenes. *Int.*
1097 *J. Nanomedicine* 2007, *2*, 639–649.
- 1098 105. Sullivan, P.D. Free radicals of benzo(a)pyrene and derivatives. *Environ. Health Perspect.* **1985**, VOL. 64,
1099 283–295, Free radicals of benzo(a)pyrene and derivatives. *Environ. Health Perspect.* 1985, VOL. 64, 283–
1100 295.
- 1101 106. Souza, T.; Jennen, D.; van Delft, J.; van Herwijnen, M.; Kyrtoupolos, S.; Kleinjans, J. New insights into
1102 BaP-induced toxicity: role of major metabolites in transcriptomics and contribution to
1103 hepatocarcinogenesis. *Arch. Toxicol.* **2016**, *90*, 1449–1458, doi:10.1007/s00204-015-1572-z.
- 1104 107. Zhang, B.; Bian, W.; Pal, A.; He, Y. Macrophage apoptosis induced by aqueous C60 aggregates changing
1105 the mitochondrial membrane potential. *Environ. Toxicol. Pharmacol.* **2015**, *39*, 237–246,
1106 doi:10.1016/j.etap.2014.11.013.
- 1107 108. Yang, L.Y.; Gao, J.L.; Gao, T.; Dong, P.; Ma, L.; Jiang, F.L.; Liu, Y. Toxicity of polyhydroxylated fullerene
1108 to mitochondria. *J. Hazard. Mater.* **2016**, *301*, 119–126, doi:10.1016/j.jhazmat.2015.08.046.
- 1109 109. Costa, P.M.; Bourgognon, M.; Wang, J.T.W.; Al-Jamal, K.T. Functionalized carbon nanotubes: From
1110 intracellular uptake and cell-related toxicity to systemic brain delivery. *J. Control. Release* **2016**, *241*, 200–

- 1111 219, doi:10.1016/j.jconrel.2016.09.033.
- 1112 110. Canesi, L.; Fabbri, R.; Gallo, G.; Vallotto, D.; Marcomini, A.; Pojana, G. Biomarkers in *Mytilus*
1113 *galloprovincialis* exposed to suspensions of selected nanoparticles (Nano carbon black, C60 fullerene,
1114 Nano-TiO₂, Nano-SiO₂). *Aquat. Toxicol.* **2010**, *100*, 168–177, doi:10.1016/j.aquatox.2010.04.009.
- 1115 111. Verghese, J.; Abrams, J.; Wang, Y.; Morano, K.A. Biology of the Heat Shock Response and Protein
1116 Chaperones: Budding Yeast (*Saccharomyces cerevisiae*) as a Model System. *Microbiol. Mol. Biol. Rev.*
1117 **2012**, *76*, 115–158, doi:10.1128/mubr.05018-11.
- 1118 112. Ryan, M.T.; Pfanner, N. Hsp70 proteins in protein translocation. *Adv. Protein Chem.* **2001**, *59*, 223–242,
1119 doi:10.1016/S0065-3233(01)59007-5.
- 1120 113. Pratt, W.B.; Toft, D.O. Regulation of Signaling Protein Function and Trafficking by the hsp90/hsp70-
1121 Based Chaperone Machinery. *Exp. Biol. Med.* **2003**, *228*, 111–133, doi:10.1177/153537020322800201.
- 1122 114. Li, J.; Zhang, Y.; Mao, F.; Tong, Y.; Liu, Y.; Zhang, Y.; Yu, Z. Characterization and Identification of
1123 Differentially Expressed Genes Involved in Thermal Adaptation of the Hong Kong Oyster *Crassostrea*
1124 *hongkongensis* by Digital Gene Expression Profiling. *Front. Mar. Sci.* **2017**, *4*, 1–12,
1125 doi:10.3389/fmars.2017.00112.
- 1126 115. Negri, A.; Oliveri, C.; Sforzini, S.; Mignione, F.; Viarengo, A.; Banni, M. Transcriptional Response of the
1127 Mussel *Mytilus galloprovincialis* (Lam.) following Exposure to Heat Stress and Copper. *PLoS One* **2013**,
1128 *8*, doi:10.1371/journal.pone.0066802.
- 1129 116. Gomes, T.; Pinheiro, J.P.; Cancio, I.; Pereira, C.G.; Cardoso, C.; Bebianno, M.J. Effects of copper
1130 nanoparticles exposure in the mussel *Mytilus galloprovincialis*. *Environ. Sci. Technol.* **2011**, *45*, 9356–9362,
1131 doi:10.1021/es200955s.
- 1132 117. Ghezzi, P.; Bonetto, V. Redox proteomics: Identification of oxidatively modified proteins. *Proteomics*
1133 **2003**, *3*, 1145–1153, doi:10.1002/pmic.200300435.
- 1134 118. Chen, S.; Qu, M.; Ding, J.; Zhang, Y.; Wang, Y.; Di, Y. BaP-metals co-exposure induced tissue-specific
1135 antioxidant defense in marine mussels *Mytilus coruscus*. *Chemosphere* **2018**, *205*, 286–296,
1136 doi:10.1016/j.chemosphere.2018.04.109.
- 1137 119. Kamat, J.P.; Devasagayam, T.P. a.; Priyadarsini, K.I.; Mohan, H.; Mittal, J.P. Oxidative damage induced
1138 by the fullerene C60 on photosensitization in rat liver microsomes. *Chem. Biol. Interact.* **1998**, *114*, 145–
1139 159, doi:10.1016/S0009-2797(98)00047-7.
- 1140 120. Kamat, J.P.; Devasagayam, T.P.A.; Priyadarsini, K.I.; Mohan, H. Reactive oxygen species mediated
1141 membrane damage induced by fullerene derivatives and its possible biological implications. *Toxicology*
1142 **2000**, *155*, 55–61, doi:10.1016/S0300-483X(00)00277-8.
- 1143 121. Xu, X.; Li, R.; Ma, M.; Wang, X.; Wang, Y.; Zou, H. Multidrug resistance protein P-glycoprotein does not
1144 recognize nanoparticle C 60: Experiment and modeling. *Soft Matter* **2012**, *8*, 2915–2923,
1145 doi:10.1039/c2sm06811g.

- 1146 122. Smital, T.; Sauerborn, R.; Hackenberger, B.K. Inducibility of the P-glycoprotein transport activity in the
1147 marine mussel *Mytilus galloprovincialis* and the freshwater mussel *Dreissena polymorpha*. *Aquat.*
1148 *Toxicol.* **2003**, *65*, 443–465, doi:10.1016/S0166-445X(03)00175-9.
- 1149 123. Xu, X.; Wang, X.; Li, Y.; Wang, Y.; Yang, L. A large-scale association study for nanoparticle C60 uncovers
1150 mechanisms of nanotoxicity disrupting the native conformations of DNA/RNA. *Nucleic Acids Res.* **2012**,
1151 *40*, 7622–7632, doi:10.1093/nar/gks517.
- 1152 124. An, H.; Jin, B. DNA exposure to buckminsterfullerene (C 60): Toward DNA stability, reactivity, and
1153 replication. *Environ. Sci. Technol.* **2011**, *45*, 6608–6616, doi:10.1021/es2012319.
- 1154 125. Park, E.J.; Roh, J.; Kim, Y.; Park, K. Induction of inflammatory responses by carbon fullerene (C60) in
1155 cultured RAW264.7 cells and in intraperitoneally injected mice. *Toxicol. Res.* **2013**, *26*, 267–273,
1156 doi:10.5487/TR.2010.26.4.267.